

Supporting information for

Micronization of CL-20 using supercritical and liquefied gases

*Mikhail N. Zharkov, Ilya V. Kuchurov, Sergei G. Zlotin**

N. D. Zelinsky Institute of Organic Chemistry, Russian Academy of Sciences,
47, Leninsky prospekt, 119991 Moscow, Russian Federation
Fax: +7 499 135 53 28; Tel: :+7 499 137 13 53.

* zlotin@ioc.ac.ru

Table of contents

1 General information	2
1.1 Materials	2
1.2 Instruments	2
2 Experimental procedures	3
2.1 Supercritical Anti-Solvent process (SAS).....	3
2.2 Gaseous Anti-Solvent process (GAS).....	5
2.3 Rapid expansion of supercritical solutions (RESS).....	8
3 Spectral data	10
4 Physical-chemical analysis.....	46
4.1 Mechanical sensitivity	46
4.2 Particle size	46
4.3 Thermal behavior	46
5 X-ray crystallographic data of α-CL-20-CO₂	48

1 General information

1.1 Materials

The initial ϵ -CL-20 powder was synthesized¹ and recrystallized² in accordance with known methods. Its structure and purity were confirmed with ^1H and ^{13}C NMR, FTIR-ATR and X-ray diffraction. The organic solvents (laboratory grade) were supplied by Acros Organics. Carbon dioxide (grades 3 and 4.5) and 1,1,1,2-tetrafluoroethane (GB/T 18826-2002) were purchased from Linde Gas (Russia).

1.2 Instruments

The ^1H and ^{13}C NMR spectra were recorded on a Bruker AM-300 (300.13 and 75.47 MHz, respectively). The FTIR-ATR spectra were obtained on Simex FT-801 spectrometer. The Raman spectra of the polymorphs were registered in the region 100–4000 cm^{-1} using a Jobin-Yvon LabRAM-300 laser Raman spectrometer with 632.8 nm excitation of a He-Ne laser with 2 mW power. The Powder X-ray diffraction patterns were recorded on Bruker D8 ADVANCE X-Ray Diffractometer (CuK_α , 40 kV, 40 mA, Ni-filter, LYNXEYE detector, reflection geometry). X-ray diffraction data were collected at 100 K on a Bruker Quest D8 diffractometer equipped with a Photon-III area-detector (graphite monochromator, shutterless ϕ - and ω -scan technique), using Mo K_α -radiation (0.71073 Å). The intensity data were integrated by the SAINT program³ and were corrected for absorption and decay using SADABS.⁴ The structure was solved by direct methods using SHELXT⁵ and refined on F^2 using SHELXL-2018.⁶ All non-hydrogen atoms were refined with individual anisotropic displacement parameters. Positions of all hydrogen atoms were found from the electron density difference map; these atoms were refined with individual isotropic displacement parameters. The SHELXTL program³ suite was used for molecular graphics.

The particle size distribution is determined by the method of dynamic laser diffraction on Analysette 22 MicroTec Plus (Fritsch) in water with the addition of a surfactant and with pre-treatment by ultrasound to separate the aggregated particles of the powder. For each component, at least five samples are taken, with each analyzed at least five times.

Differential scanning calorimetry (DSC) was registered in separate experiments in Netzsch DSC 204 HP apparatus.

¹ N.V. Latypov, U. Wellmar, P. Goede, A.J. Bellamy. *Org. Process Res. Dev.*, **2000**, 4(3), 156-158.

² J.H. Urbelis, J.A. Swift. *Cryst. Growth Des.*, **2014**, 14(4), 1642-1649.

³ Bruker. APEX-III. *Bruker AXS Inc.*, Madison, Wisconsin, USA, 2019.

⁴ L. Krause, R. Herbst-Irmer, G.M. Sheldrick, D. Stalke. *J. Appl. Cryst.* **2015**, 48, 3–10.

⁵ G.M. Sheldrick. *Acta Cryst.* **2015**, A71, 3-8.

⁶ G.M. Sheldrick. *Acta Cryst.* **2015**, C71, 3-8.

2 Experimental procedures

2.1 Supercritical Anti-Solvent process (SAS)

The scheme of the installation for SAS experiments is shown on Figure 1.

Carbon dioxide supplied to the system from the cylinder **1** is being pre-cooled in the thermostat **2** to avoid further cavitation. Then, the liquefied CO₂ is being transported by high-pressure pump **3** through the thermostat (heater) **4** into the temperature-controlled autoclave with the precipitation chamber **5** of 500 cm³ volume. The thermostat **4** heats the constantly incoming fluid to the required temperature. The pressure inside the system is maintained with the automated back pressure regulator (ABPR) **9**. The initial solution of CL-20 is being fed from the reservoir **6** with the plunger pump **7** to the filled with sc-CO₂ autoclave **5** through the sapphire nozzle **8** in the lid. The mutual diffusion of CO₂ and organic solvent results in the precipitation of CL-20 particles which are being collected on the metallic filter at the bottom of the precipitation chamber. The binary mixture CO₂-solvent leaves the autoclave and goes through ABPR **9** and is being divided inside the separator **10** at a lower pressure controlled with the manual back pressure regulator (MBPR) **11**.

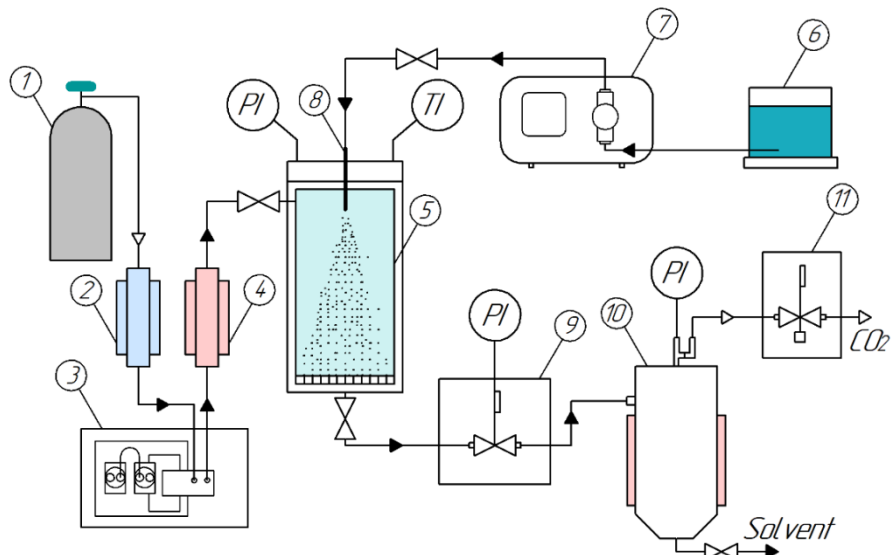


Figure 1. SAS process setup: **1** – cylinder with CO₂; **2** – thermostat (cooler); **3** – high pressure pump; **4** – thermostat (heater); **5** – precipitation chamber with fine filter at the bottom; **6** – beaker with CL-20 solution in organic solvent; **7** – solution pump; **8** – sapphire nozzle; **9** – automated back pressure regulator; **10** – separator; **11** – manual back pressure regulator.

General procedure. The experimental conditions are shown in the Table 1. First, the system is filled with CO₂ at the constant flow rate (50 g/min) and thermostated. Once the required values of pressure and temperature are achieved the CL-20 solution in organic solvent

starts to flow with the low rate (1-4 mL/min) into the precipitation chamber through the nozzle. After the solution is fully transferred into the autoclave, the CO₂ feeding continues for extra 30 min to wash out the organic solvent residues. The process being finished, the system is decompressed, and the solid product is taken out.

Table 1. Experimental conditions for SAS processing of CL-20.

No	Solvent	Temperature, °C	Pressure, MPa	CL-20 solution conc., % mass.	CL-20 solution flow rate, mL/min	Product crystal phase
1	Ethyl acetate	40	20	2	2	α
2	-//-	40	20	5	1	α
3	-//-	40	30	10	1	α
4	-//-	40	20	10	2	α
5	-//-	40	10	10	1	α
6	-//-	80	10	10	1	- ^a
7	-//-	40	30	10	4	α
8	Acetone	40	20	10	2	α
9	Acetonitrile	40	20	10	1	- ^a
10	Propylene carbonate	40	20	10	1	- ^a

^a The product was washed out from precipitation chamber.

2.2 Gaseous Anti-Solvent process (GAS)

The principal scheme of the GAS experimental setup is depicted on Figure 2. Two different fluids were used for the process as the anti-solvent: CO₂ and TFE (lines **a** and **b** correspondingly).

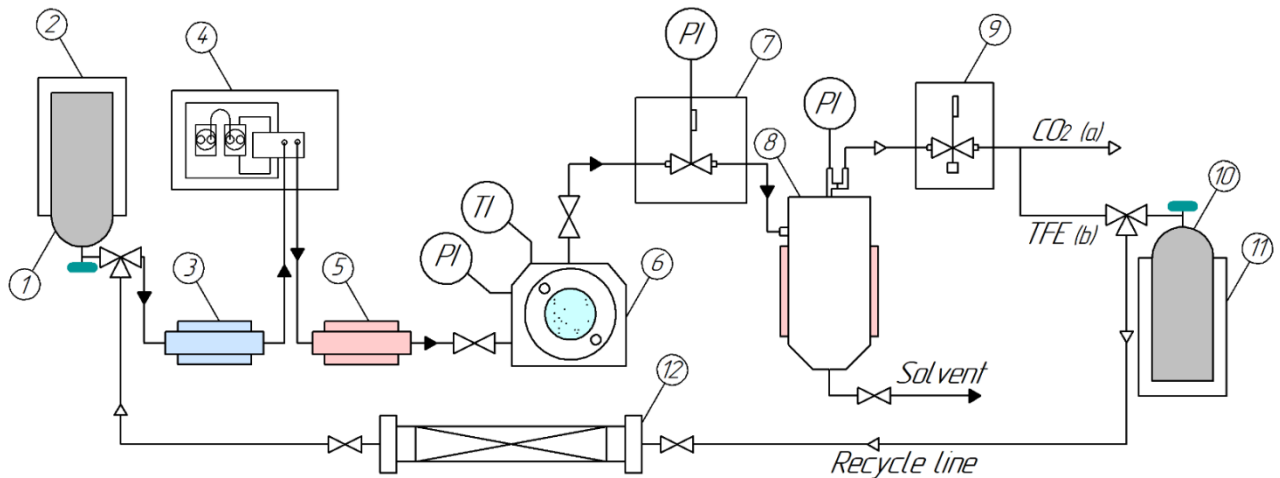


Figure 2. GAS process setup: **a** – the CO₂-based setup; **b** – the TFE-based setup.
1 – cylinder with CO₂ or TFE; **2,11** – cylinder heating/cooling jacket; **3** – thermostat (cooler); **4** – high pressure pump; **5** – thermostat (heater); **6** – precipitation chamber; **7** – automated back pressure regulator; **8** – separator; **9** – manual back pressure regulator; **10** – cylinder for TFE accumulation; **12** – sorption tube.

Liquefied gas (CO₂ or TFE) from the cylinder **1** is pre-cooled in the thermostat **3** and enters the high-pressure pump **4** which delivers it with strict flow rate control through the heater **5** into the temperature-controlled precipitation chamber **6** of 22 cm³ volume. The precipitation chamber **6** is equipped with a stirrer and two looking-through sapphire glasses and filled with a portion of CL-20 solution of a given concentration in an organic solvent. At the constant stirring the CL-20 solution expands with the gas being delivered into the chamber **6**, and after the saturation point is reached CL-20 particles start to precipitate. The addition of the fluid continues until the suspension fills whole volume and the pressure reaches slightly heightened setpoint on the automated back pressure regulator (ABPR) **7**. Then the solvents binary mixture is being washed out by passing the fresh liquefied gas flow (25 ml /min) through the precipitation chamber **6**. Then the flow is being divided on organic solvent and gas in the heat-assisted separator **8** at a lower pressure controlled by MBPR **9**. If the TFE is used as the working medium in the setup (line **b**) then the gas from the separator **8** heads into the cylinder **10** cooled with thermostat **11** at -10°C where it being condensed for reuse. To ensure that no

organic vapors are accumulated in recycled TFE it could be re-condensed through the sorption tube **12** filled with activated carbon.

General procedure. The experimental conditions are shown in the Table 2 (CO_2) and Table 3 (TFE). The precipitation chamber is preliminary filled with the CL-20 solution (4 mL) of certain concentration in an organic solvent, and sealed. Then the required temperature is achieved the anti-solvent (CO_2 or TFE) is being added with the certain flow rate. The CL-20 particles start to precipitate when the chamber is nearly 60% filled with the mixture of solvents, that can be seen through the sapphire windows. The anti-solvent addition continues until the autoclave is totally filled and further for some extra pressure (10 MPa and 1 MPa for CO_2 and TFE correspondingly) which is maintained by ABPR to assure the continuity of the medium. The fresh anti-solvent washes out the binary mixture from the precipitation chamber at the constant pressure and flow rate (25 mL/min) into the separator. After that, the process is stopped, the chamber is decompressed, and the product is taken out.

Table 2. Experimental conditions for GAS processing of CL-20 in CO_2 medium.

No	Solvent	Solution conc., % mass.	CO_2 flow rate, ^a ml/min	Temperature, °C	CL-20 crystal phase
1	Ethyl acetate	15	5	30	α
2	-/-	15	5	40	α
3	-/-	15	5	50	α
4	-/-	10	5	40	α
5	-/-	5	0.5	40	
6	-/-	5	2	40	α
7	-/-	5	5	40	α
8	-/-	5	7	40	α
9	-/-	5	10	40	α
10	-/-	5	25	40	α
11	-/-	5	5	80	α
12 ^b	-/-	5	5	40	α
13*	-/-	5	5	60	α
14	Acetone	5	10	40	α
15	Acetone	10	25	40	α
16	Acetone	25	25	40	α
17	Acetonitrile	5	5	40	α

^a Precipitation chamber filling rate.

^b Extra-dry ethyl acetate and CO_2 of Grade 4.5 were used to perform the experiment in moisture-free conditions

Table 3. Parameters TFE-based GAS process for CL-20 micronization.

Nº	Solution conc., % mass.	TFE flow rate, ml/min	Temperature, °C	CL-20 crystal phase^c
1	1	3	20	ε
2	1	10	20	ε
3	3	1	20	ε
4	3	5	20	ε
5	3	7	20	ε
6	3	10	20	ε
7	5	0.7	20	ε
8	5	0.7	40	ε
9	5	0.7	50	ε
10	5	0.7	60	ε
11	5	1	20	ε
12 ^b	5	3	20	ε
13	5	5	20	ε
14 ^b	5	5	20	ε
15 ^b	5	5	20	ε
16 ^b	5	5	50	ε
17	5	10	20	ε
18	5	10	20	ε
19	5	10	40	ε
20	7	1	20	ε
21 ^b	7	3	20	ε
22	7	5	20	ε
23 ^b	7	5	20	ε
24	7	7	20	ε
25	7	7	50	ε+β
26 ^b	7	8	20	ε+β
27 ^b	7	8	50	ε+β
28	7	10	20	β
29 ^b	7	10	20	β
30	7	10	50	β
31 ^b	8.5	3	20	ε
32 ^b	8.5	3	20	ε
33	8.5	7.5	20	β+ε
34	8.5	7.5	50	β
35	10	1	20	ε
36	10	5	20	ε+β
37	10	5	50	β+ε
38	10	7	20	β+ε
39	10	7	50	β
40	10	10	20	β

^a Precipitation chamber filling rate.^b The raw-CL-20 was in α phase and ethyl acetate was after simple distillation were used.^c The proportion of β phase is approximate and indicated only for evaluative purposes.

2.3 Rapid expansion of supercritical solutions (RESS)

The RESS TFE-based system designed, constructed, and used in this work is shown schematically in Figure 3.

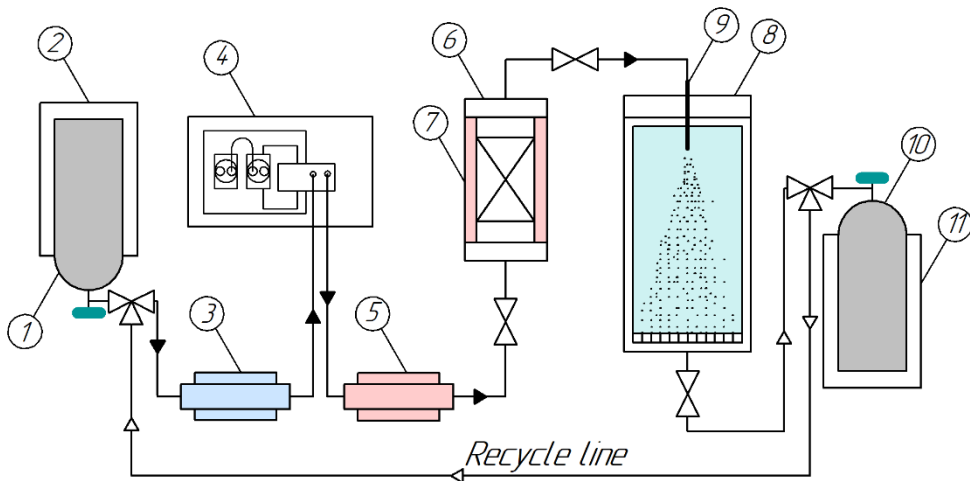


Figure 3. RESS process setup: **1,10** –cylinder with TFE; **2,11** – cylinder heating/cooling jacket; **3** – thermostat (cooler); **4** – liquid TFE pump; **5** – thermostat (heater); **6** – autoclave-extractor with CL-20; **7** – heating jacket; **8** – precipitation chamber with fine filter at the bottom; **9** – sapphire nozzle.

TFE is stored in cylinders **1** and **10** equipped with thermostat **2** and **11**. Cylinders are used interchangeably, one as a source of fluid and the other as a vessel for condensation of the used gas during the process. The thermostat **2** is designed to protect the cylinder **1** from freezing during gas intake. The other thermostat **11**, on the contrary, cools the collection vessel **10** to ensure effective condensation gaseous TFE. From the upside-downed cylinder **1** the liquefied in cooler **3** TFE enters the pump **4** which delivers it through the heater **5** into the temperature-controlled autoclave-extractor **6** (of 10 mL volume) with preloaded CL-20 (~1 g). The extractor **6** is equipped with thermostat **7** and fine filter at the outlet. The obtained at the given values of pressure and temperature CL-20 solution in TFE is being sprayed through the sapphire nozzle **9** into the temperature-controlled precipitation chamber **8** (of 500 mL volume) where pressure is much lower (~0.1-0.3 MPa) than inside the extractor. Due to the pressure drop (evaporation of TFE), the dissolved CL-20 precipitates as microcrystals on the fine filter at the bottom of the chamber **8**. TFE goes through the filter and condenses in the collecting cylinder **10** at -10°C. The high pressure inside the extractor is provided by confined carrying capacity of the nozzle along with sufficient TFE flow rate. The pressure inside the heated precipitation chamber is quasi-equal to the pressure in cooled receiving cylinder. This design

allowed conducting the micronization RESS process in a constant flow process with the only need to refill the extractor and unload the precipitation chamber.

General procedure. The autoclave-extractor containing the sample of CL-20 (1 g) was sealed and heated to required temperature. TFE pump was set in pressure mode in which it maintains the set pressure value by regulating the fluid flow. At temperatures of 40-70°C and the nozzle diameters of 100-200 μm TFE flow rates were of 50-90 g/min to maintain the pressure inside the extractor within range of 50-250 bar. When the process was finished, the pump was switched off and the precipitation chamber was decompressed and opened. In all experiments only β -CL-20 particles of similar morphology were obtained.

3 Spectral data

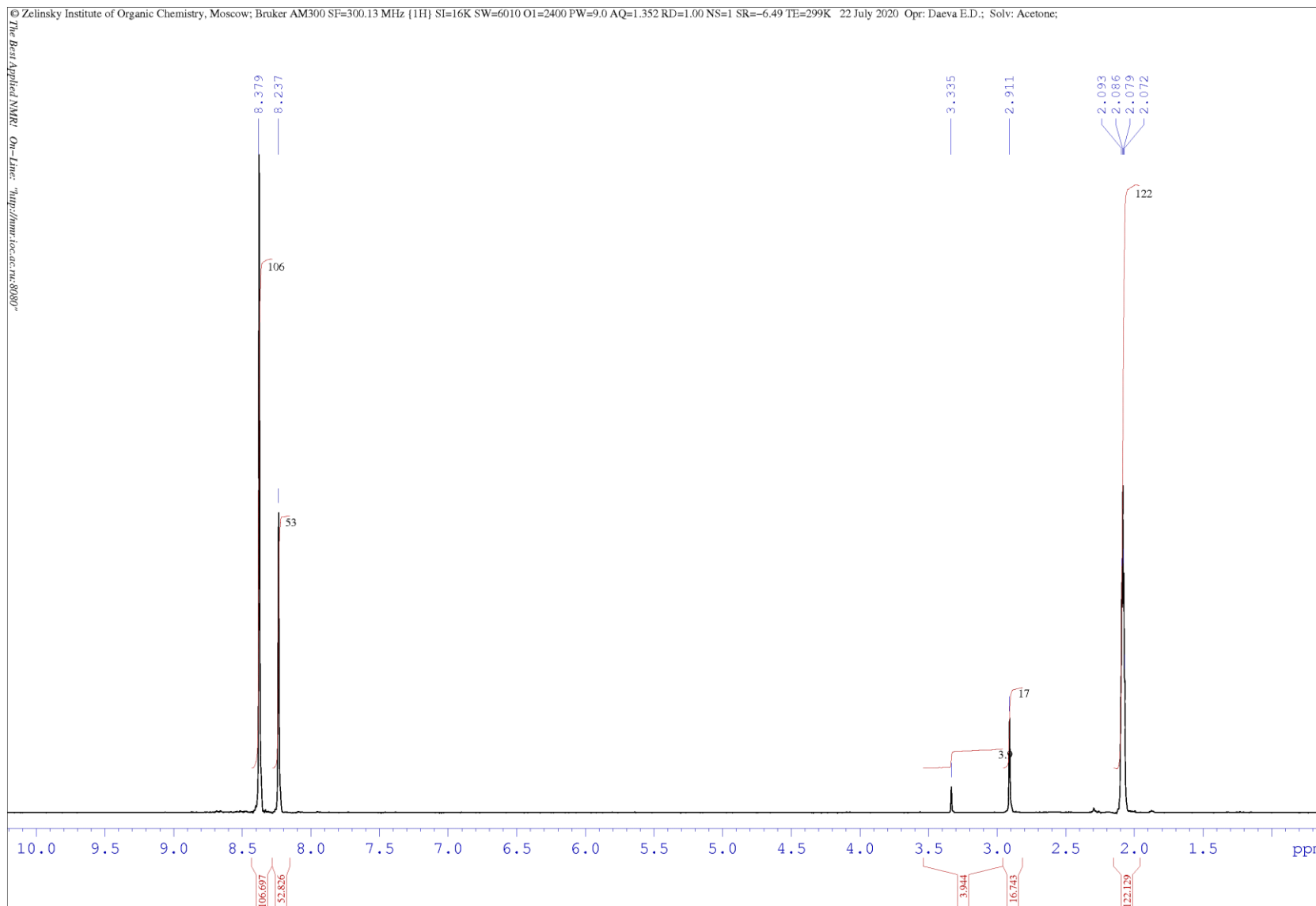
The FTIR spectra were obtained on Simex FT-801 spectrometer with an ATR accessory (ZnSe). All the spectra are given in three different scales (3200-600, 1700-600, and 1100-600 cm⁻¹) which provide the whole picture and the detailed information on the characteristic region. The spectra of ϵ -CL-20 contain four characteristic absorption bands at 737, 743, 750 and 757 cm⁻¹ and two bands at 819 and 830 cm⁻¹ of average intensity. The spectra of α -CL-20 are characterized by three absorption bands at 739, 750 and 763 cm⁻¹ and two bands at 824 and 834 cm⁻¹. β -Phase of CL-20 was identified by four absorption bands at 735, 745, 758, and 765 cm⁻¹, and a single band at 834 cm⁻¹. The obtained FTIR spectra are in agreement with the reported data for pure polymorphs.⁷ The mixed samples contain the clear distinct signals of each crystal phase due to the recording of FTIR-ATR spectra at high resolution mode (up to 1 cm⁻¹).

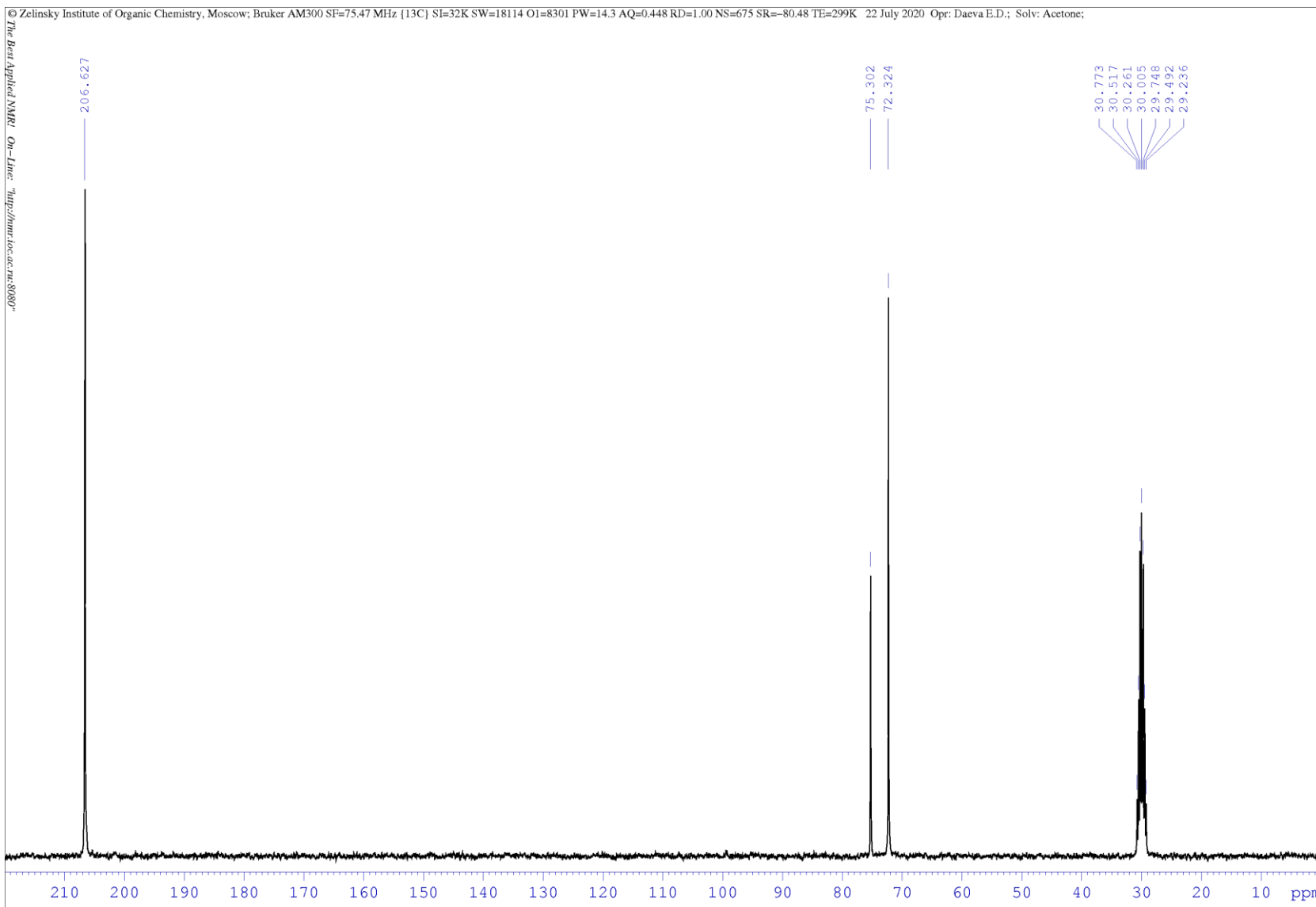
The Raman spectra of the polymorphs were recorded on Jobin-Yvon LabRAM-300 laser Raman spectrometer (632.8 nm excitation of a He-Ne laser with 2 mW power). The spectrum of ϵ -CL-20 contains intensive characteristic peak at 344 cm⁻¹, the spectrum of β -phase of CL-20 has the characteristic peak at 281 cm⁻¹. Both peaks are in agreement with reported data for corresponding polymorphs⁸.

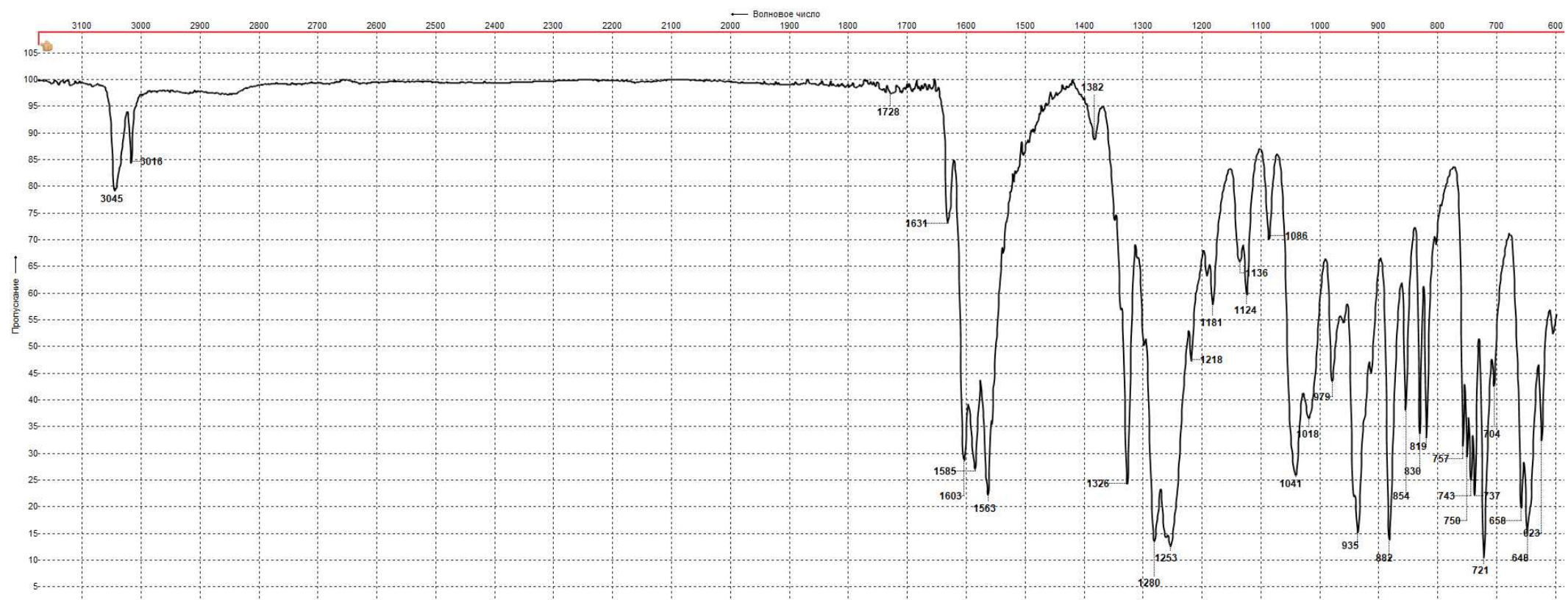
The powder X-ray diffraction patterns were recorded for β - and ϵ -CL-20 on Bruker D8 ADVANCE X-Ray Diffractometer (CuK _{α} 40kV, 40 mA, filter, LYNXEYE detector, reflection geometry). The obtained spectra of the individual polymorphs and their mixtures well corresponded with data from the Cambridge Crystallographic Data Centre (CCDC).

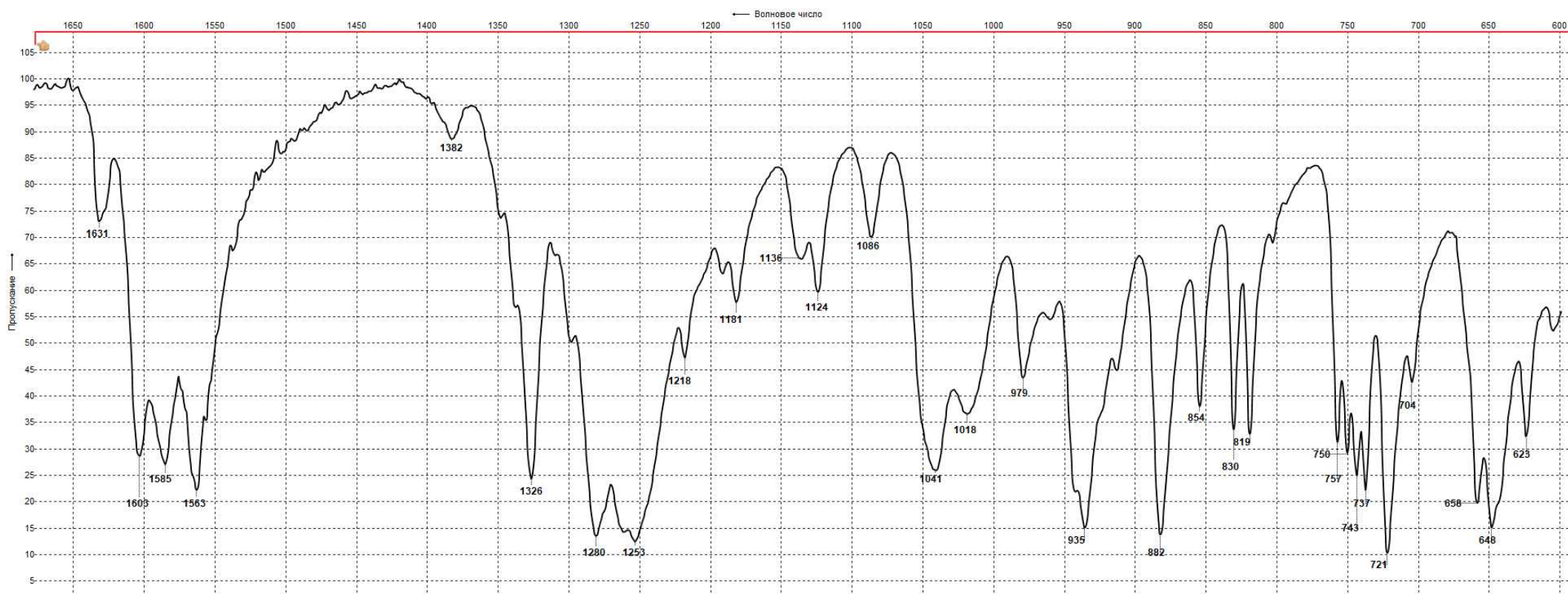
⁷ M. Ghosh, V. Venkatesan, S. Mandave, S. Banerjee, N. Sikder, A.K. Sikder, B. Bhattacharya. *Cryst. Growth Des.*, **2014**, *14*(10), 5053-5063.

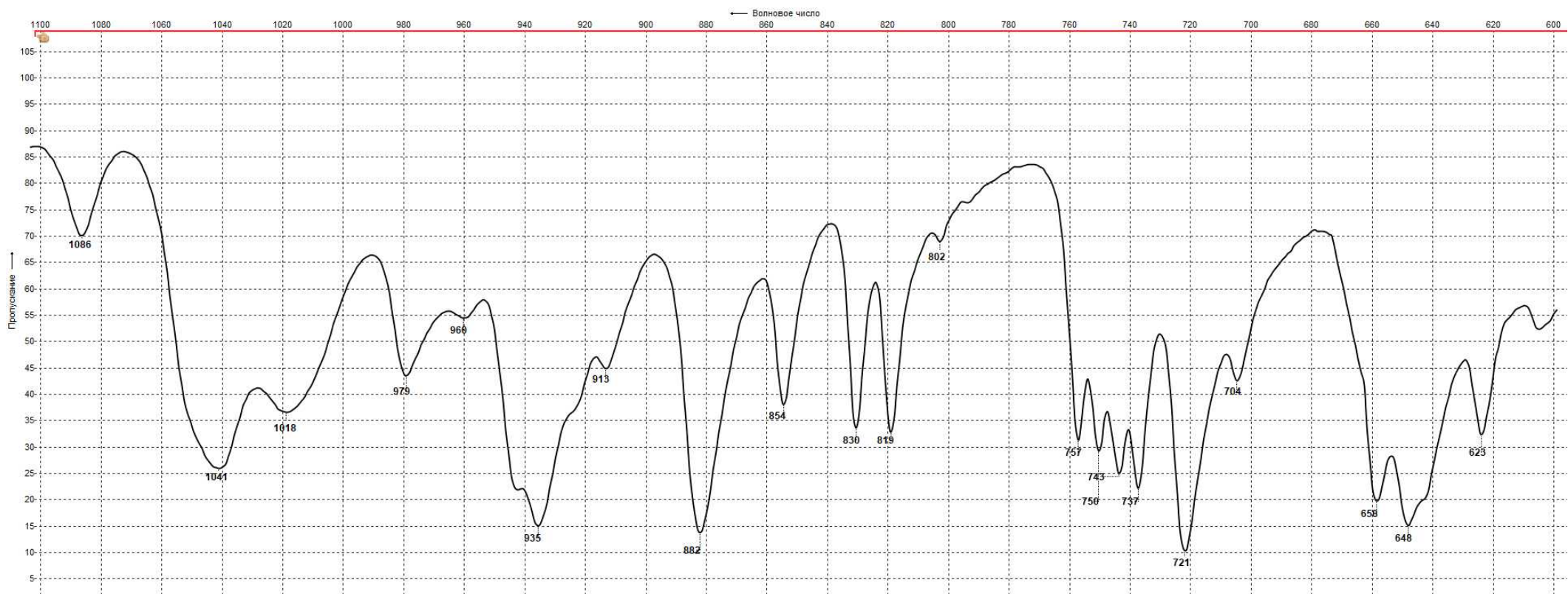
⁸ M. Ghosh, S. Banerjee, M. A. Shafeeuulla Khan, N. Sikder and A. K. Sikder, *Phys. Chem. Chem. Phys.*, **2016**, *18*, 23554–23571.

¹H NMR spectrum of initial CL-20

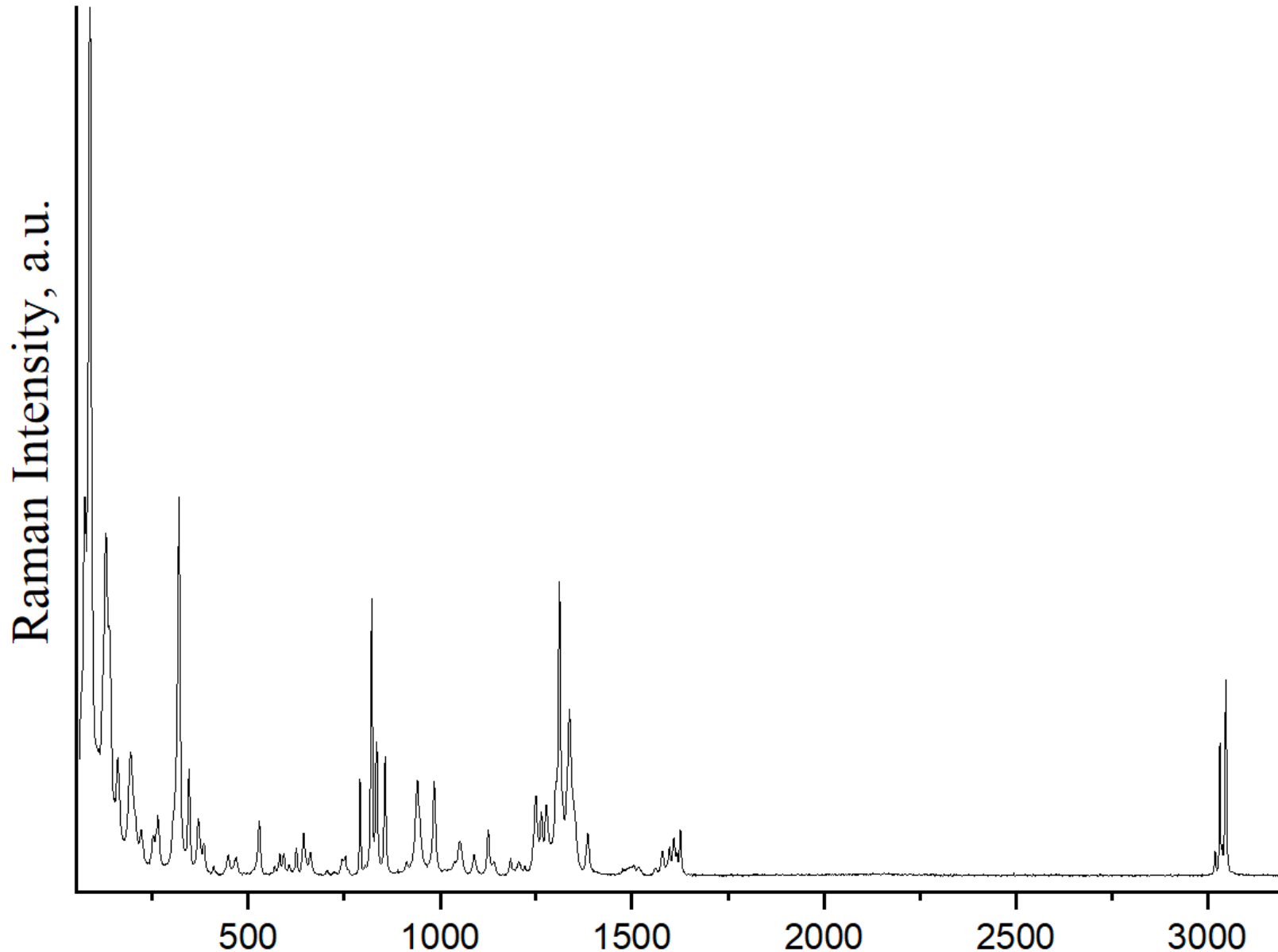
¹³C NMR spectrum of initial CL-20

FTIR-ATR spectrum of initial ϵ -CL-20 (3200-600 cm⁻¹ range)

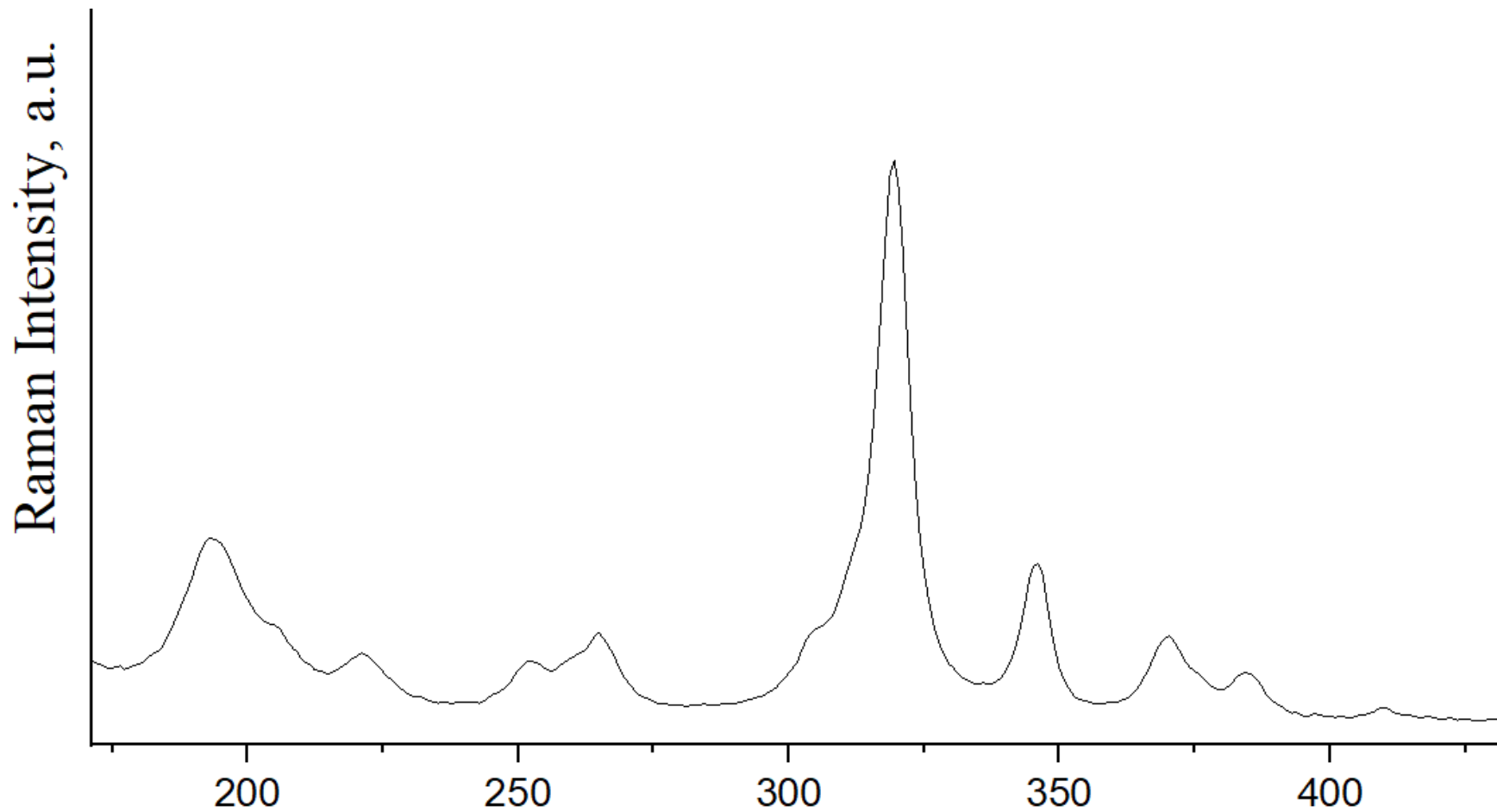
FTIR-ATR spectrum of initial ϵ -CL-20 (1700-600 cm^{-1} range)

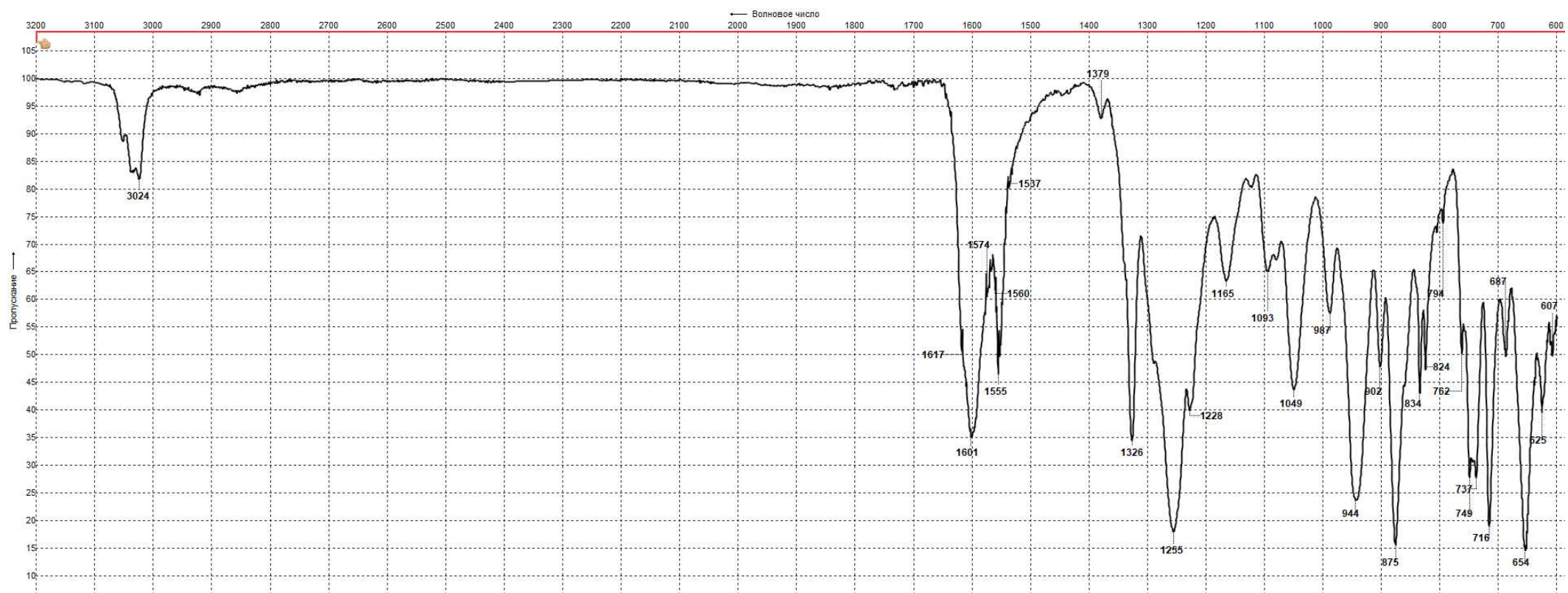
FTIR-ATR spectrum of initial ϵ -CL-20 (1100-600 cm^{-1} range)

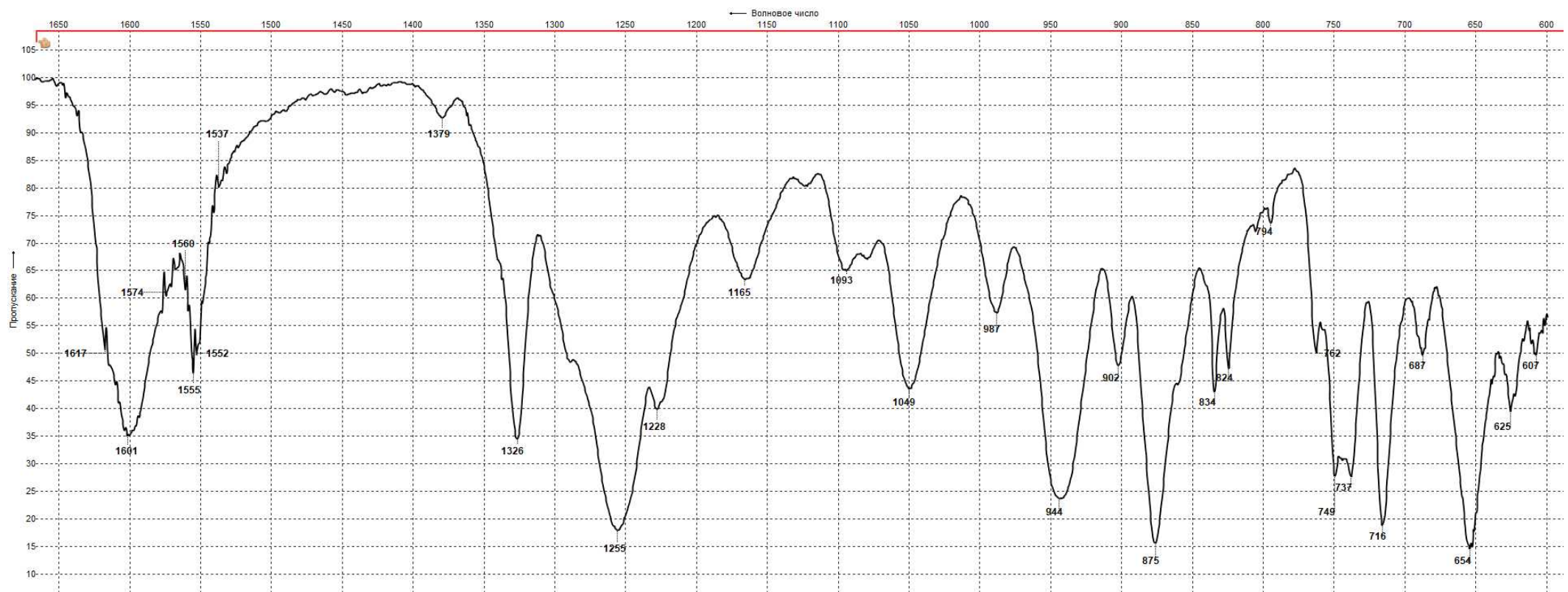
Raman spectrum of initial ϵ -CL-20 (0-3500 cm^{-1} range)

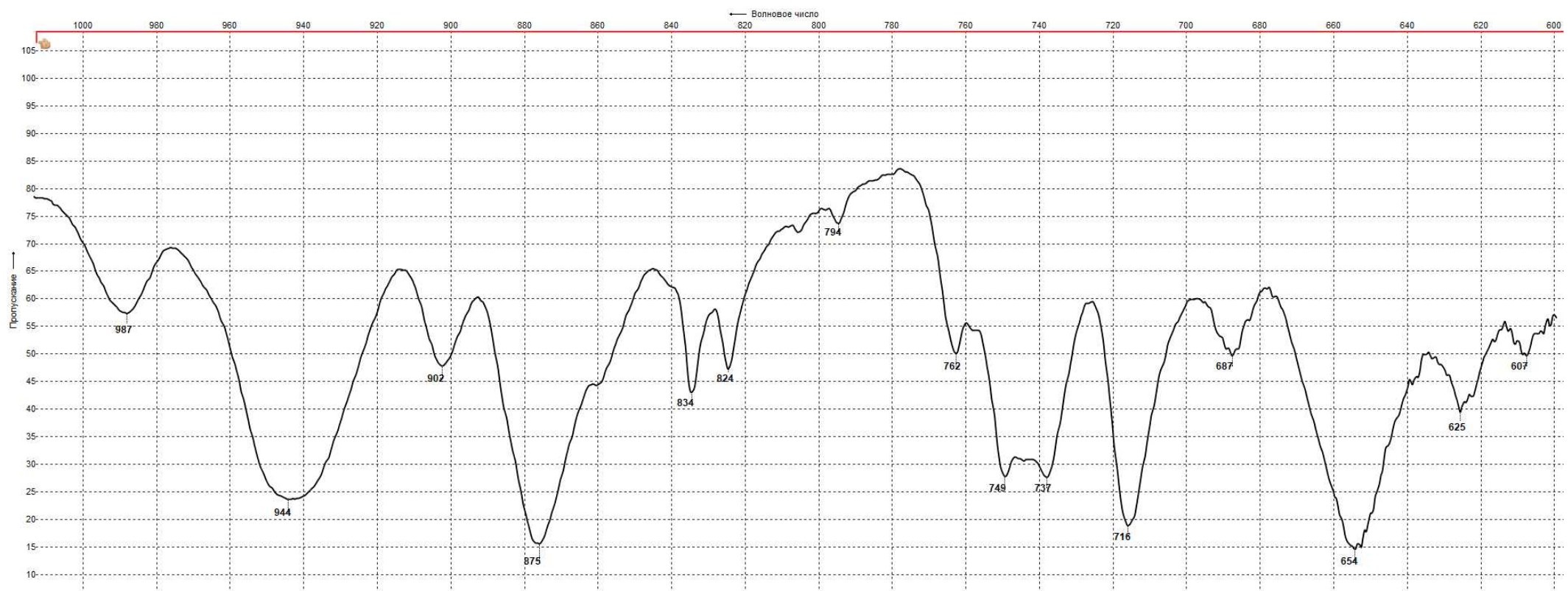


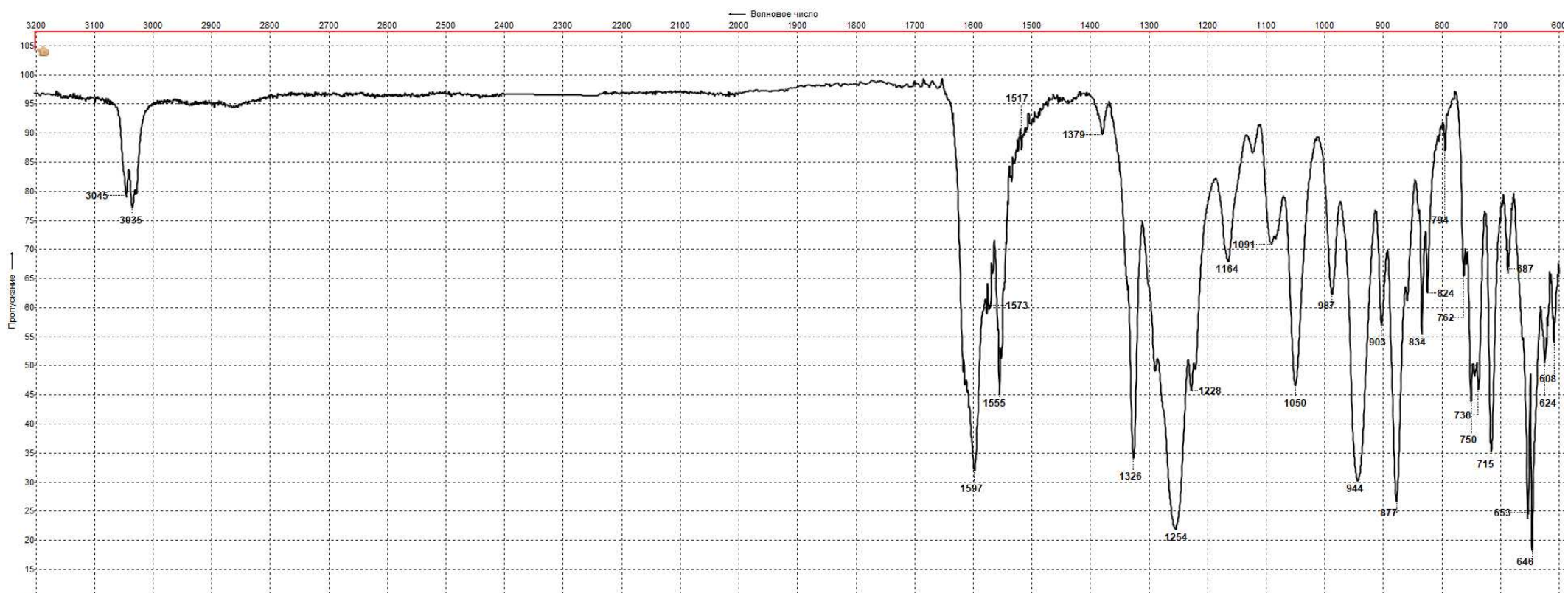
Raman spectrum of initial ε -CL-20 (200-400 cm^{-1} range)

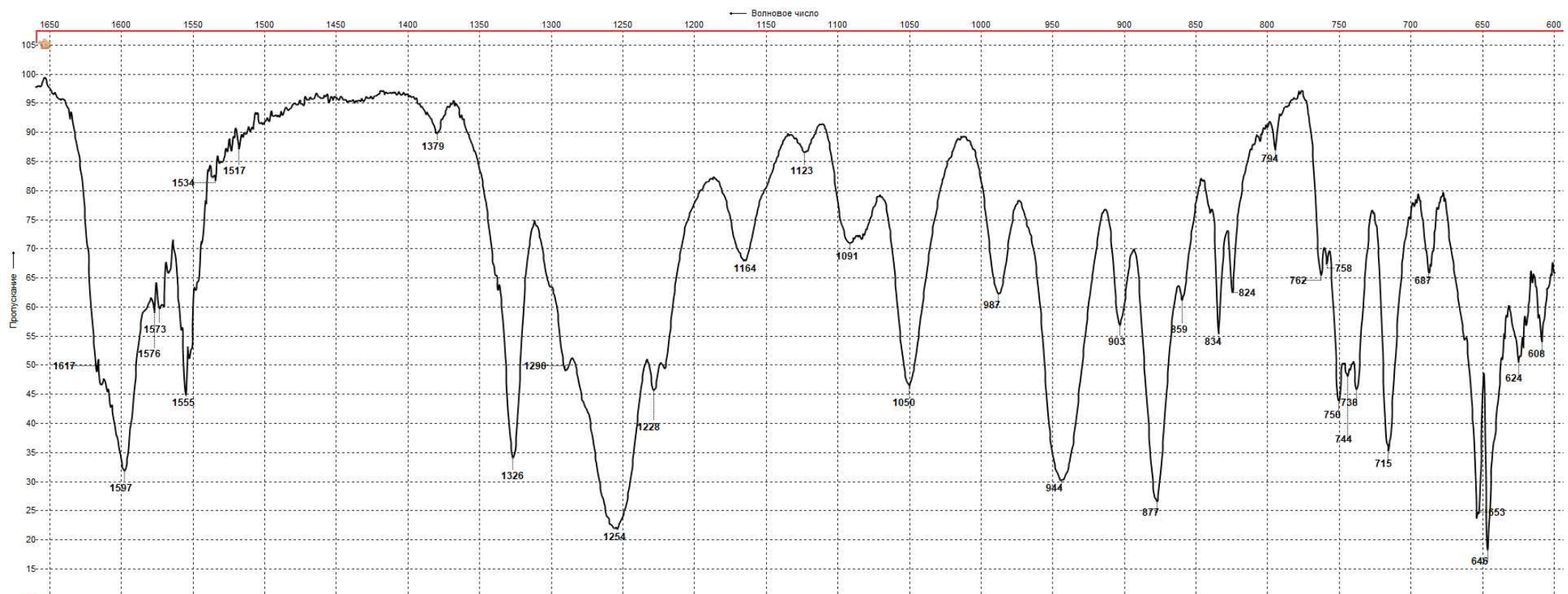


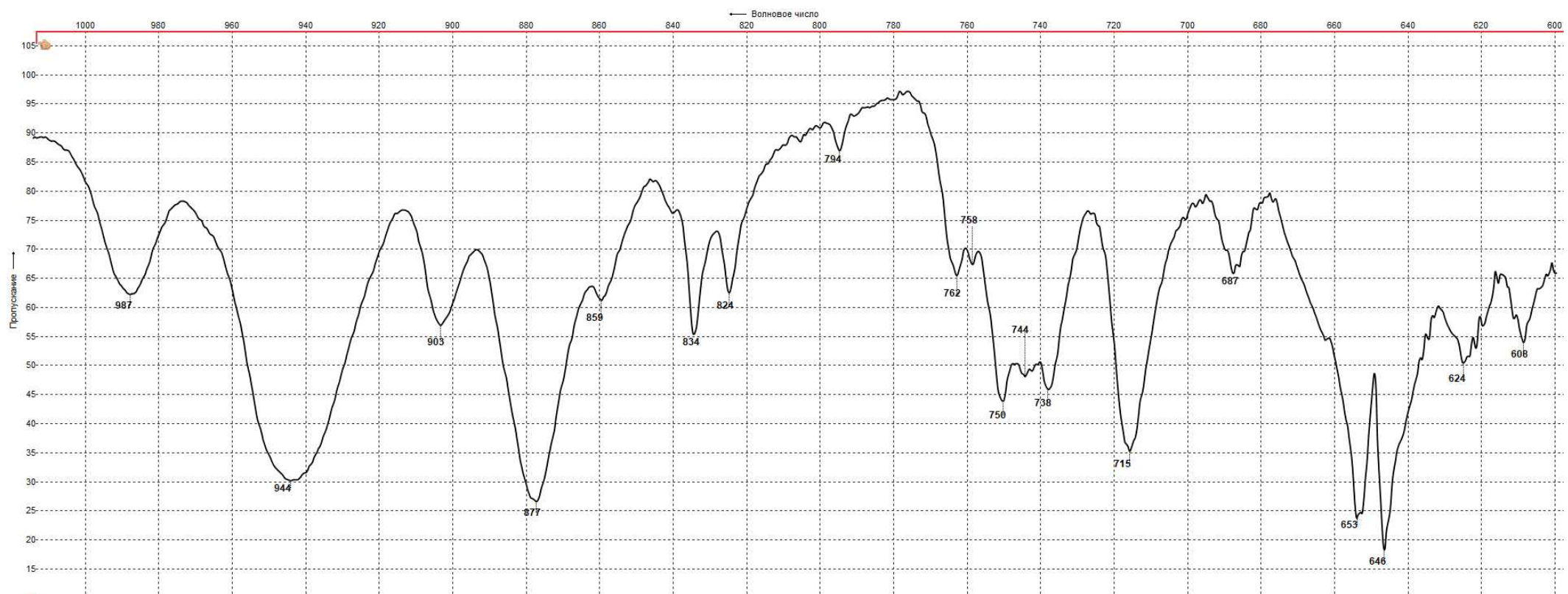
FTIR-ATR spectrum of α -CL-20 (3200-600 cm^{-1} range)

FTIR-ATR spectrum of α -CL-20 (1700-600 cm^{-1} range)

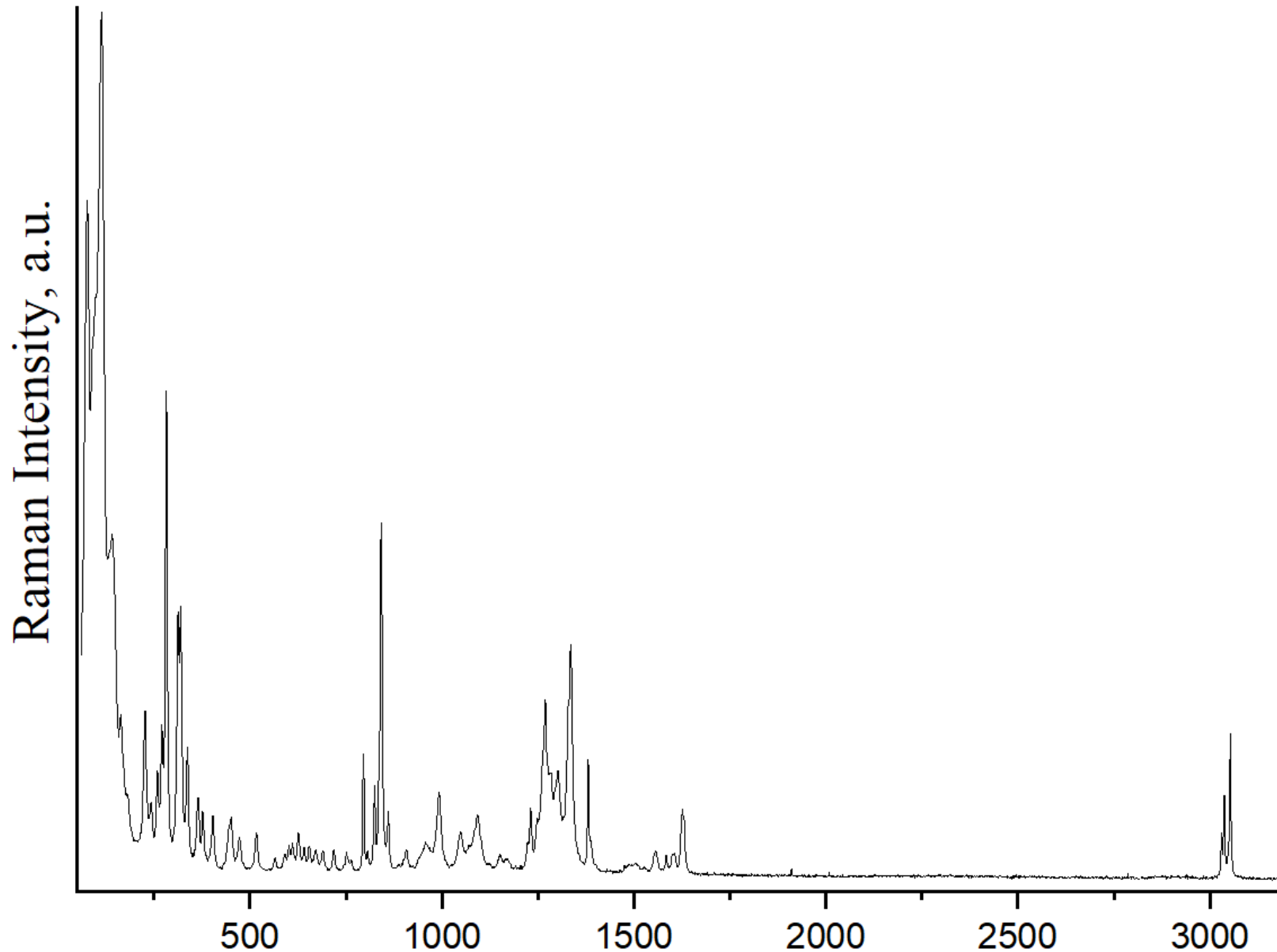
FTIR-ATR spectrum of α -CL-20 (1100-600 cm⁻¹ range)

FTIR-ATR spectrum of α -CL-20-CO₂ (3200-600 cm⁻¹ range)

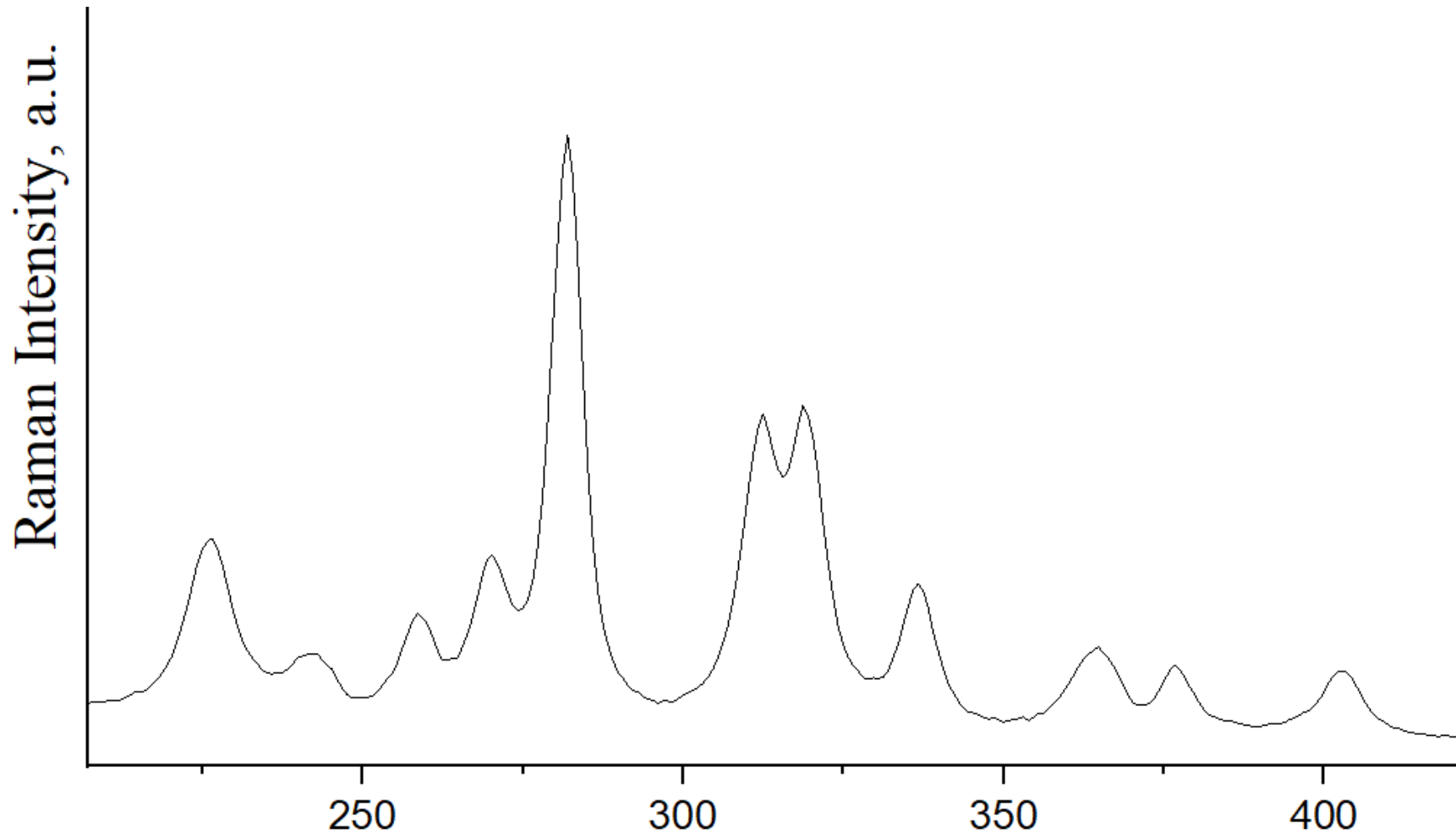
FTIR-ATR spectrum of α -CL-20-CO₂ (1700-600 cm⁻¹ range)

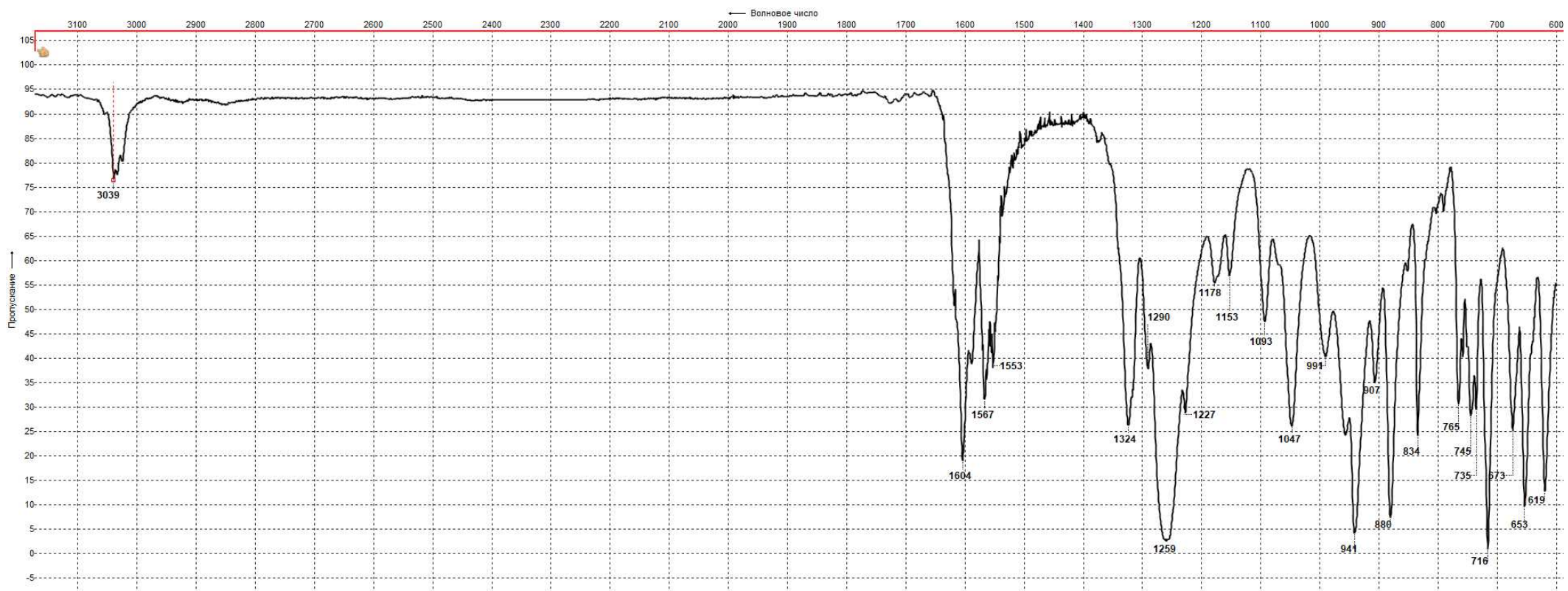
FTIR-ATR spectrum of α -CL-20-CO₂ (1100-600 cm⁻¹ range)

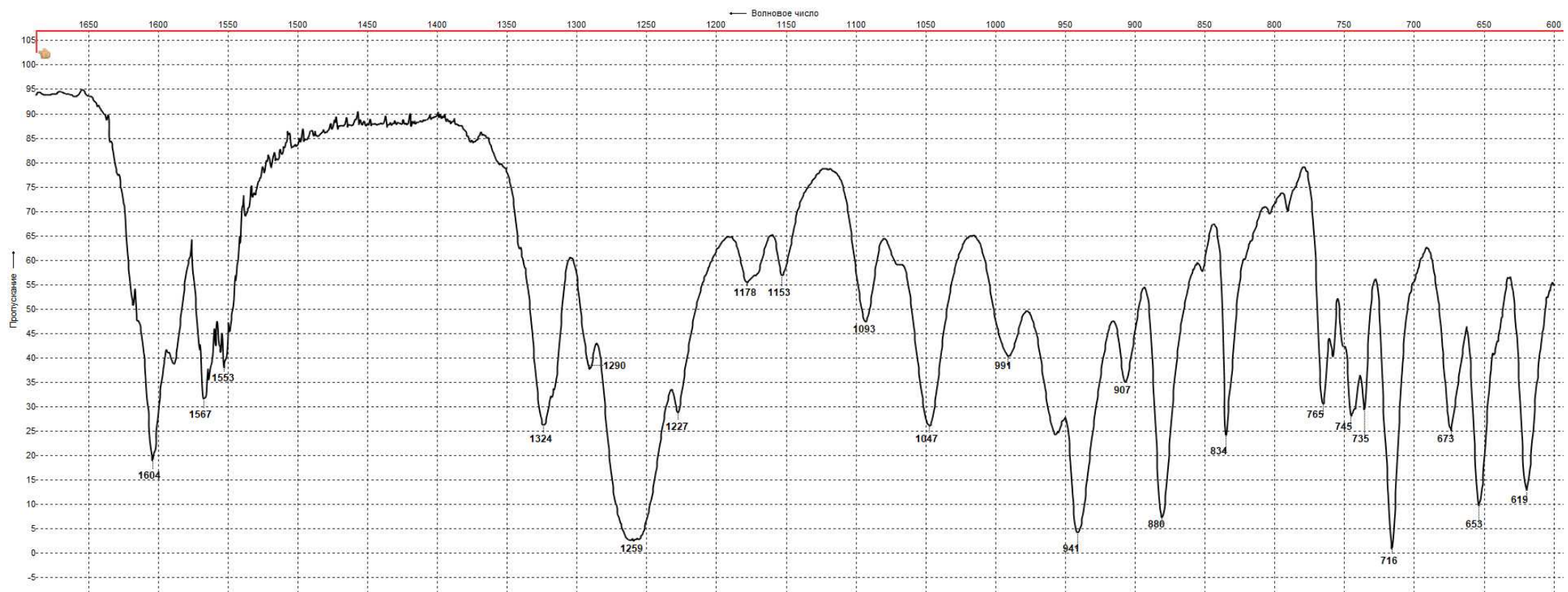
Raman spectrum of α -CL-20-CO₂ (0-3500 cm⁻¹ range)



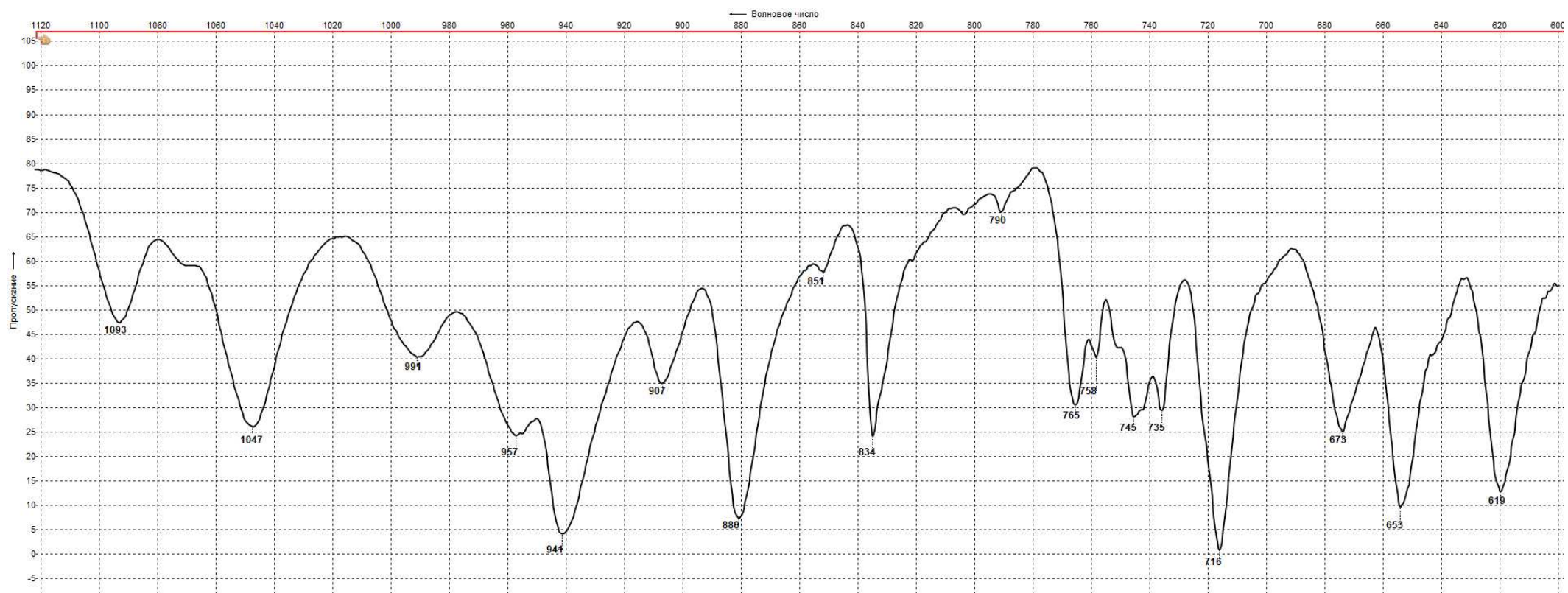
Raman spectrum of α -CL-20-CO₂ (200-400 cm⁻¹ range)



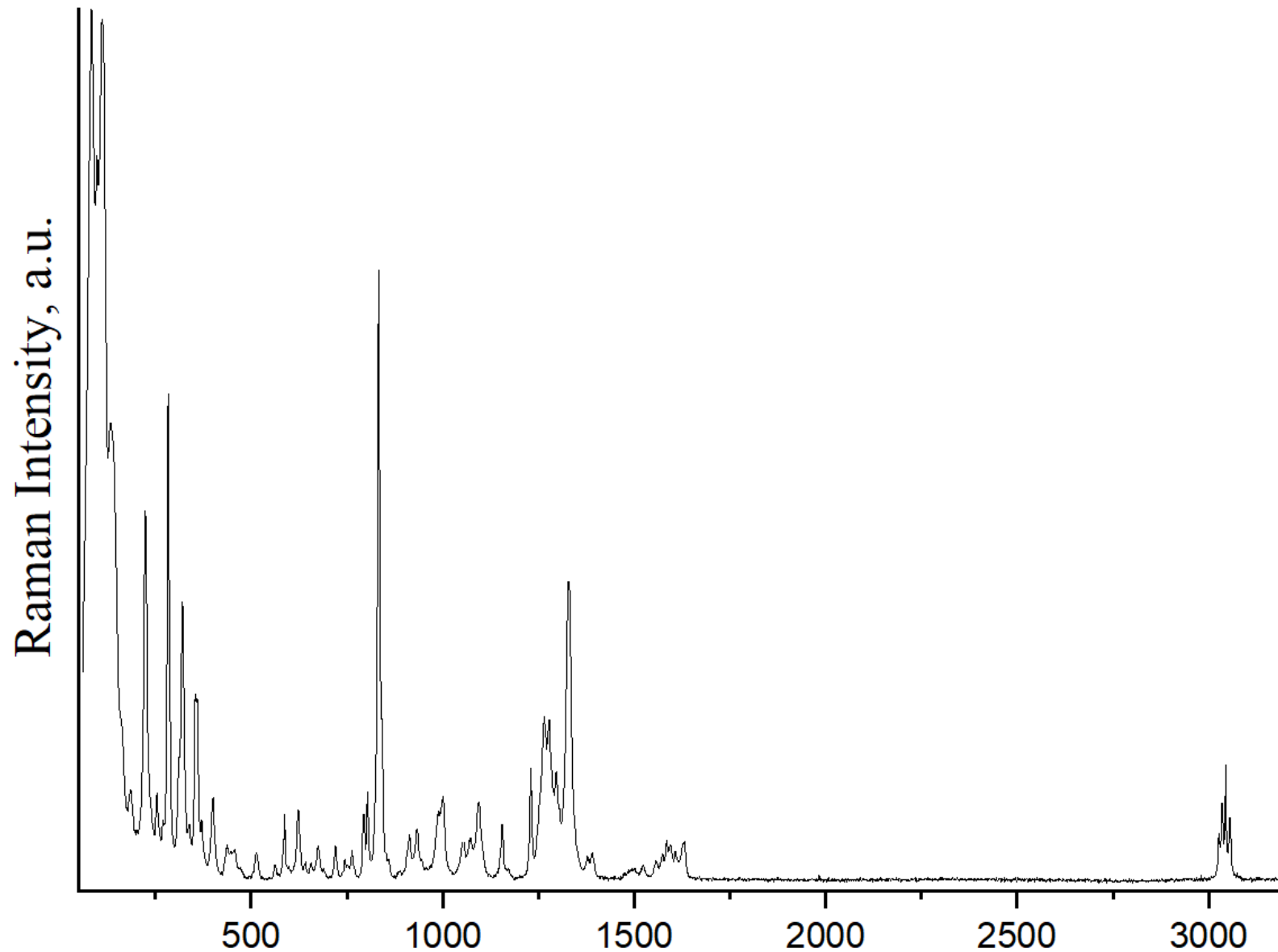
FTIR-ATR spectrum of β -CL-20 (3200-600 cm^{-1} range)

FTIR-ATR spectrum of β-CL-20 (1700-600 cm⁻¹ range)

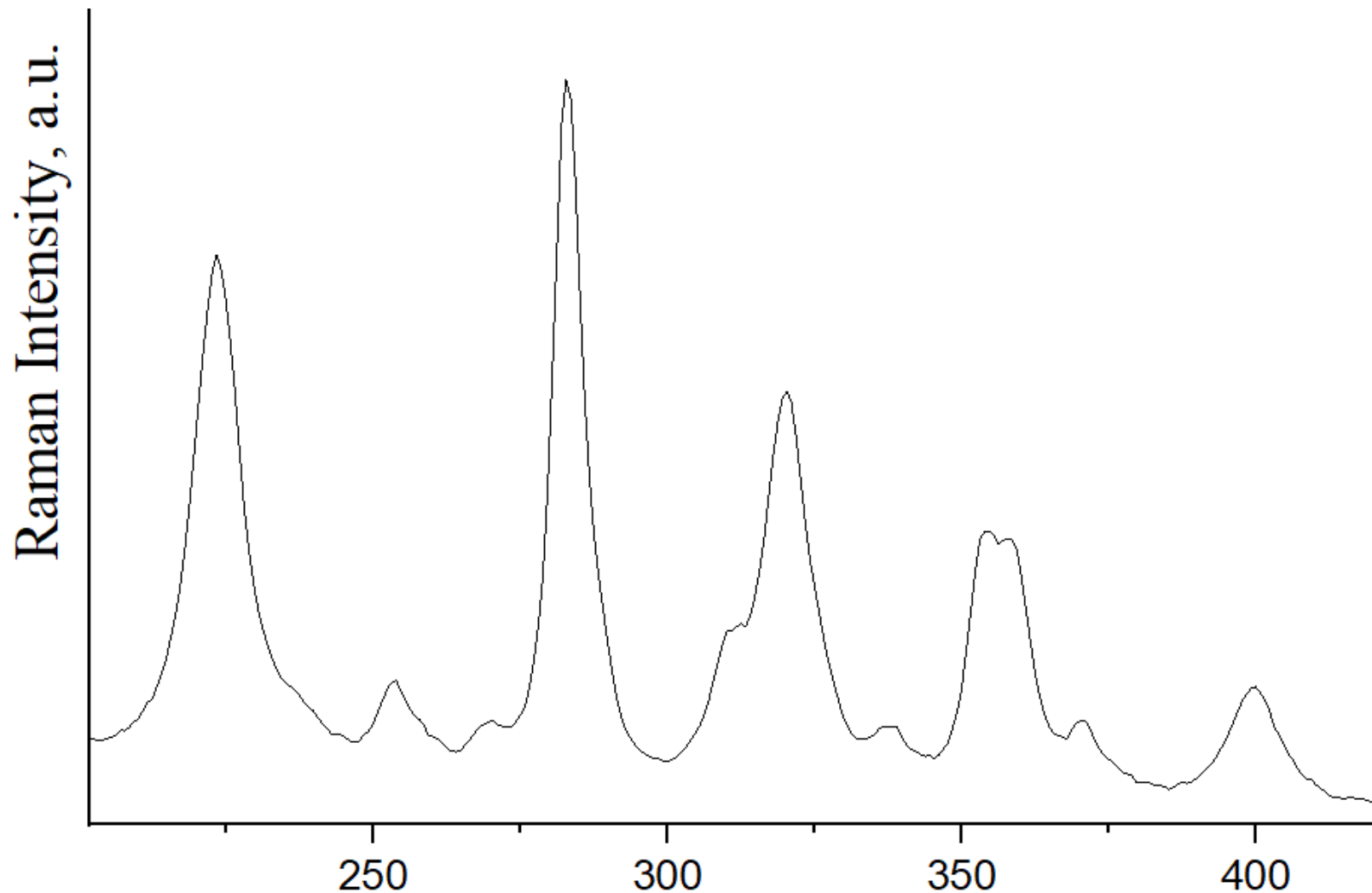
FTIR-ATR spectrum of β -CL-20 (1100-600 cm⁻¹ range)

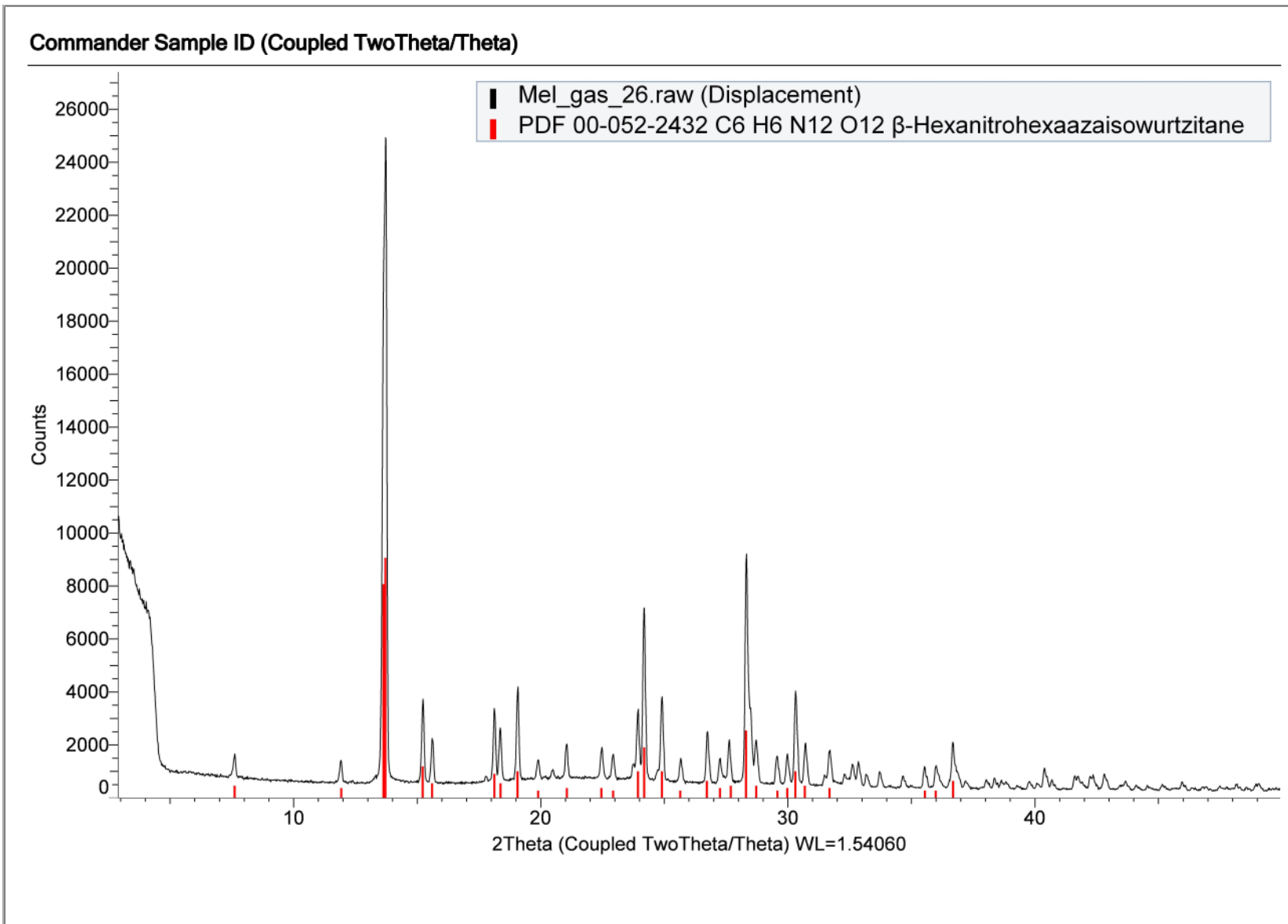


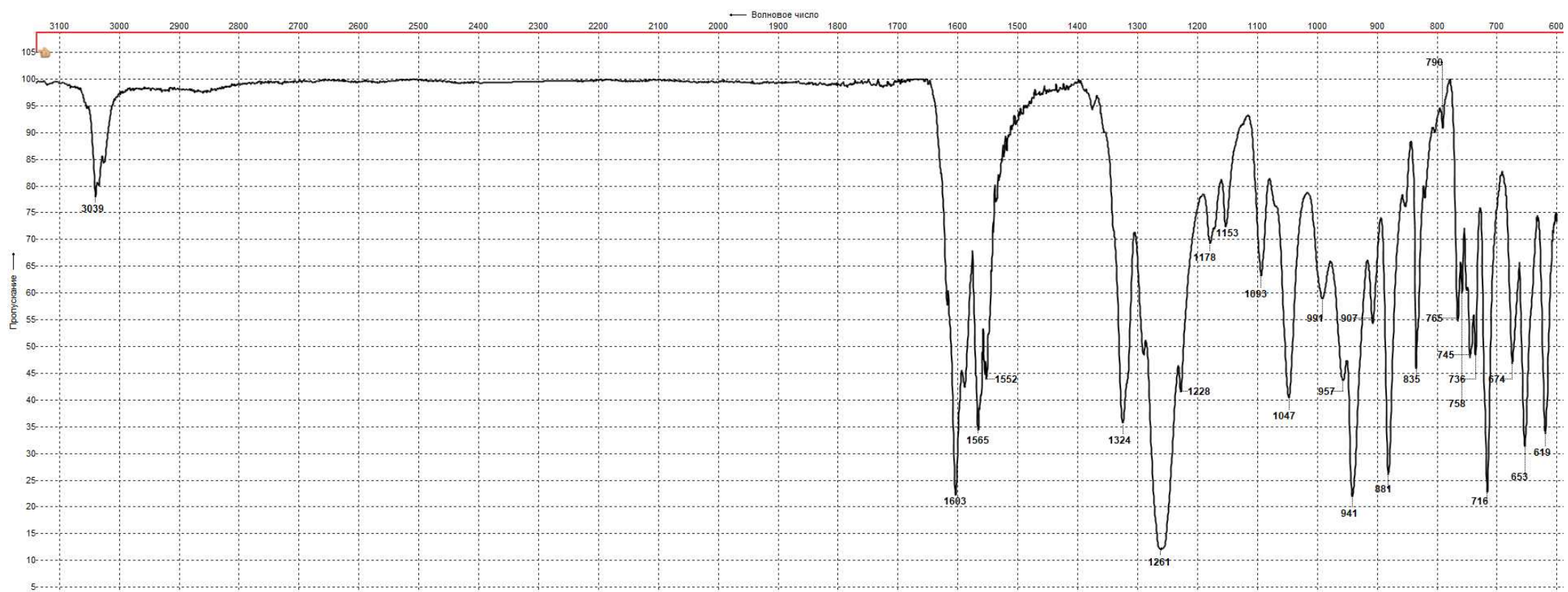
Raman spectrum of β -CL-20 (0-3500 cm^{-1} range)



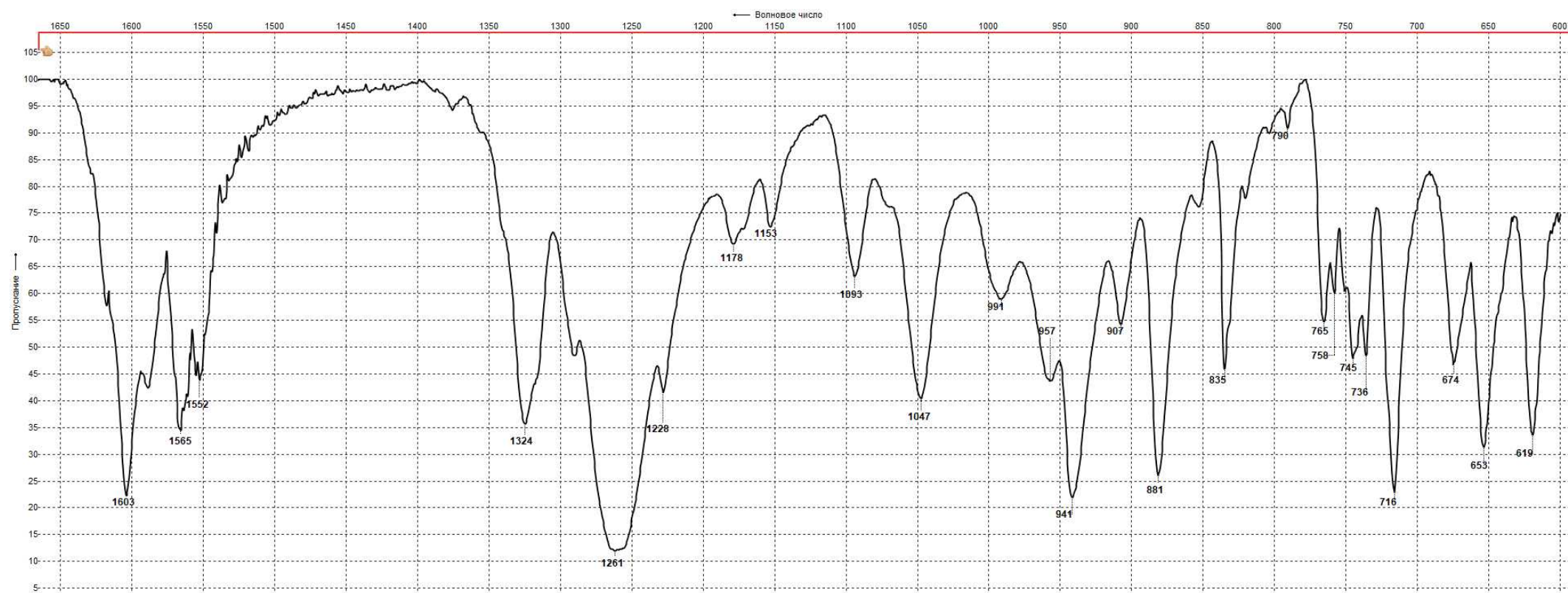
Raman spectrum of β -CL-20 (200-400 cm $^{-1}$ range)

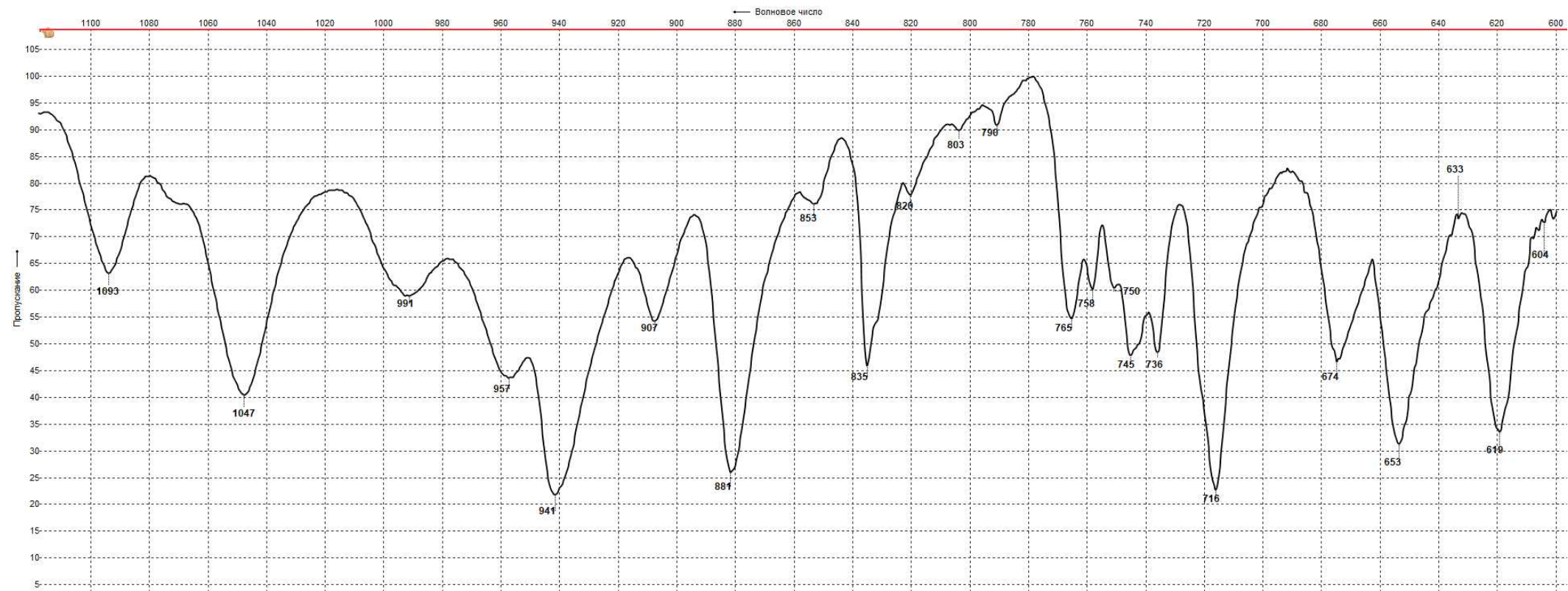


The Powder X-ray diffractogram of β -CL-20

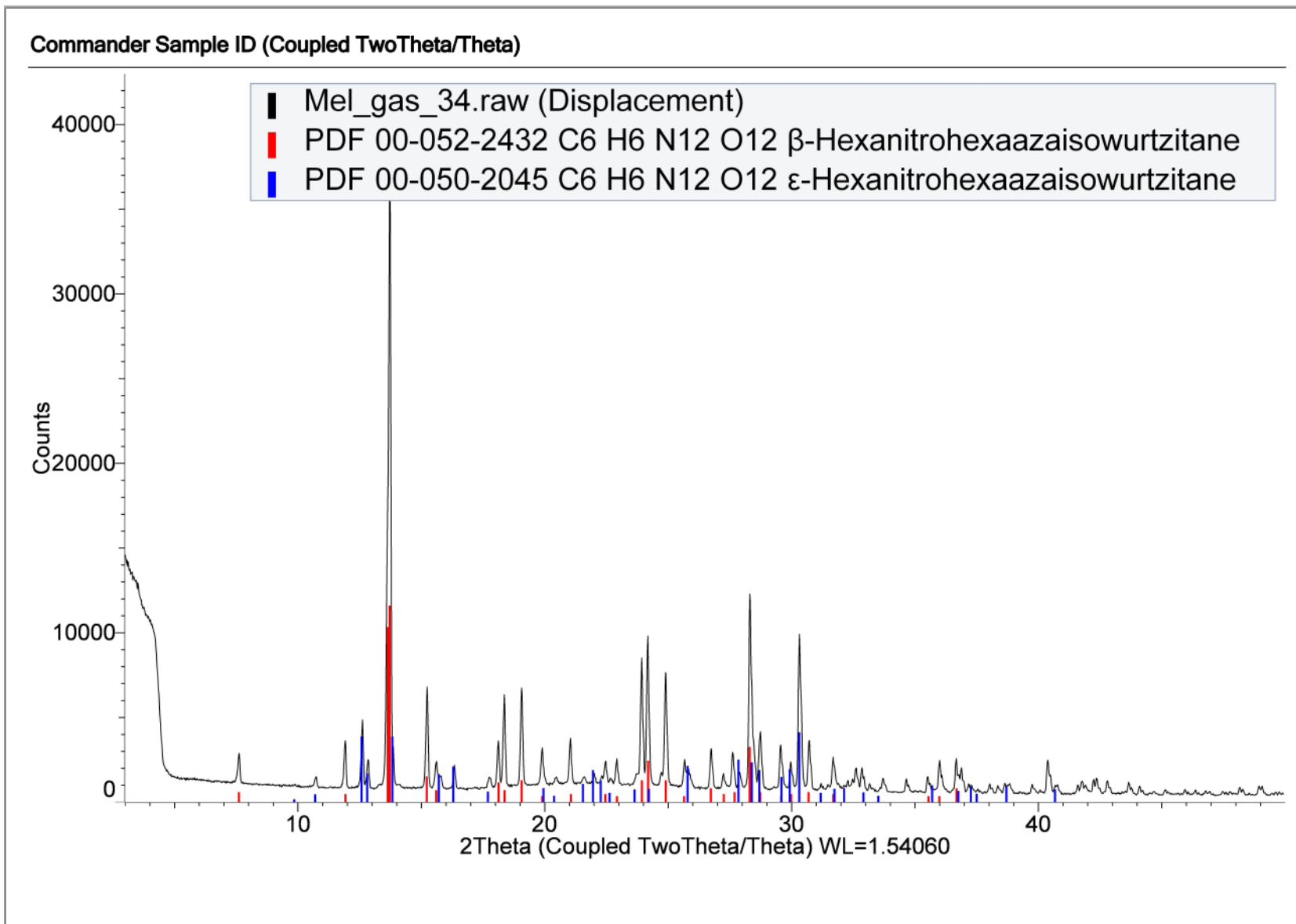
FTIR-ATR spectrum of mixture β -CL-20 with ε -CL-20 (3200-600 cm^{-1} range)

FTIR-ATR spectrum of mixture β -CL-20 with ε -CL-20 (31700-600 cm^{-1} range)

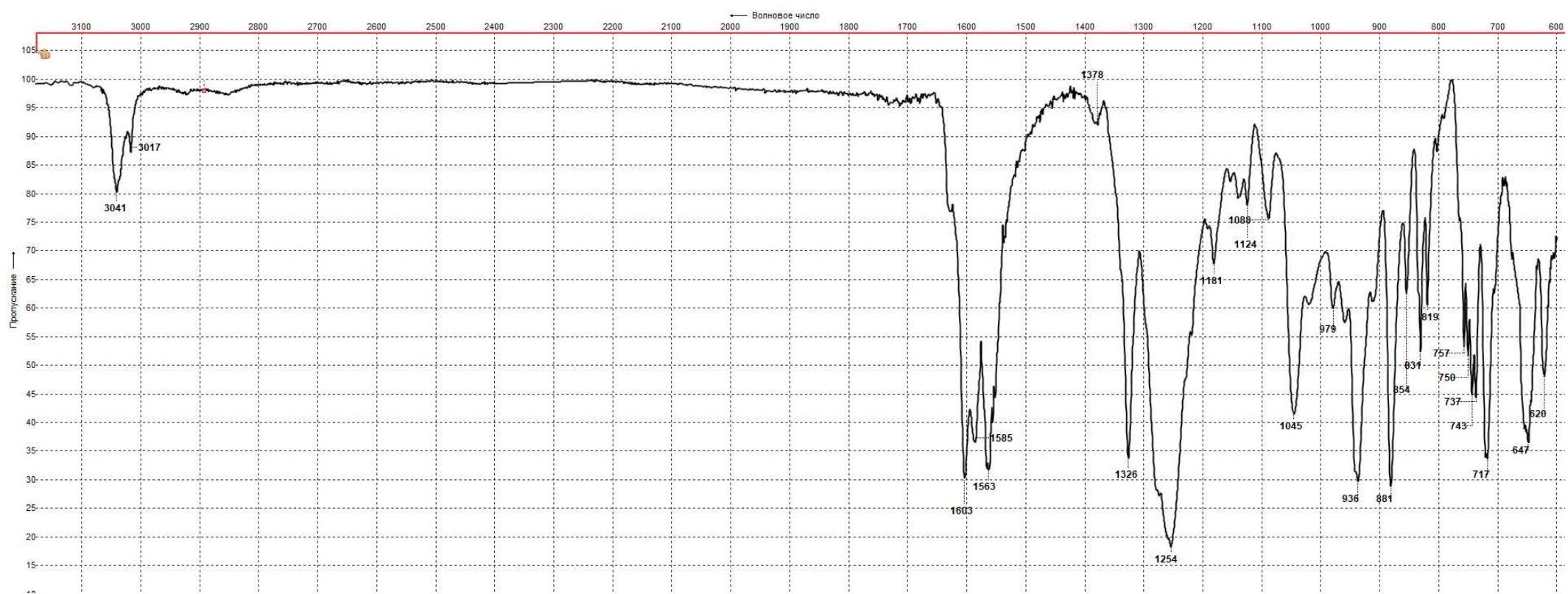


FTIR-ATR spectrum of mixture β -CL-20 with ε -CL-20 (1100-600 cm⁻¹ range)

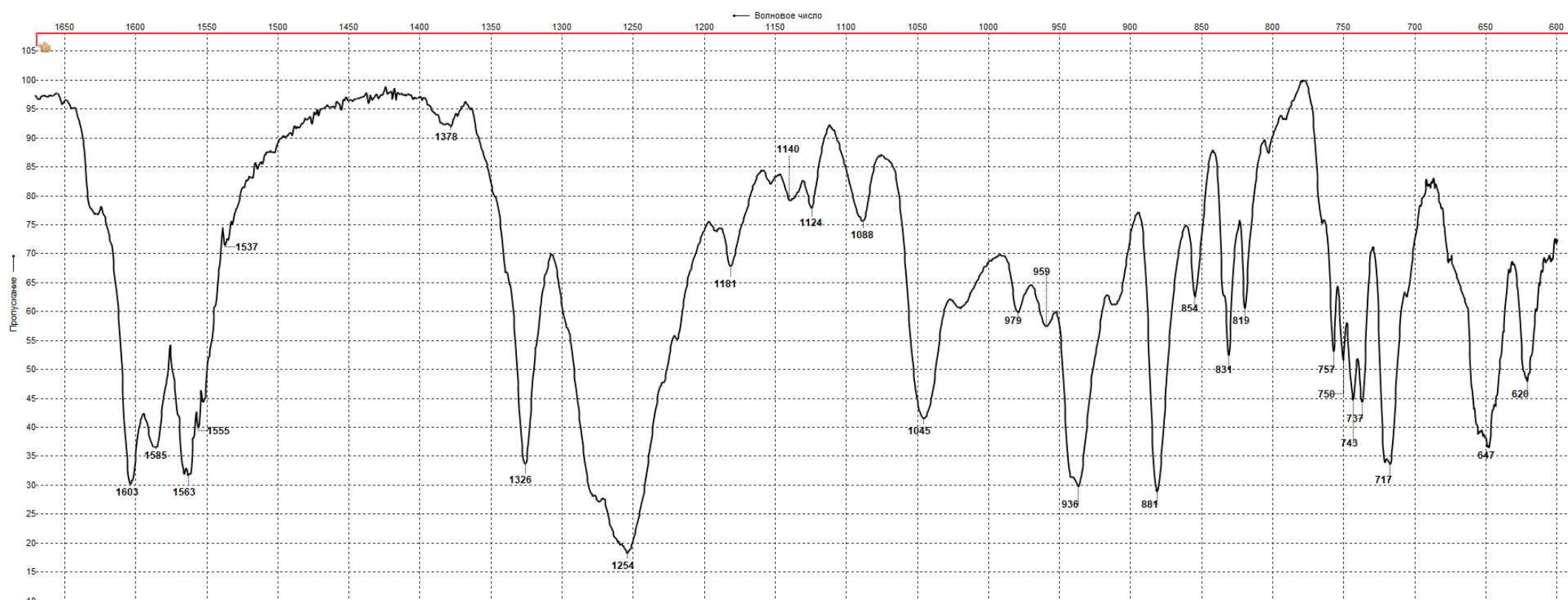
The Powder X-ray diffractogram of mixture β -CL-20 with ϵ -CL-20



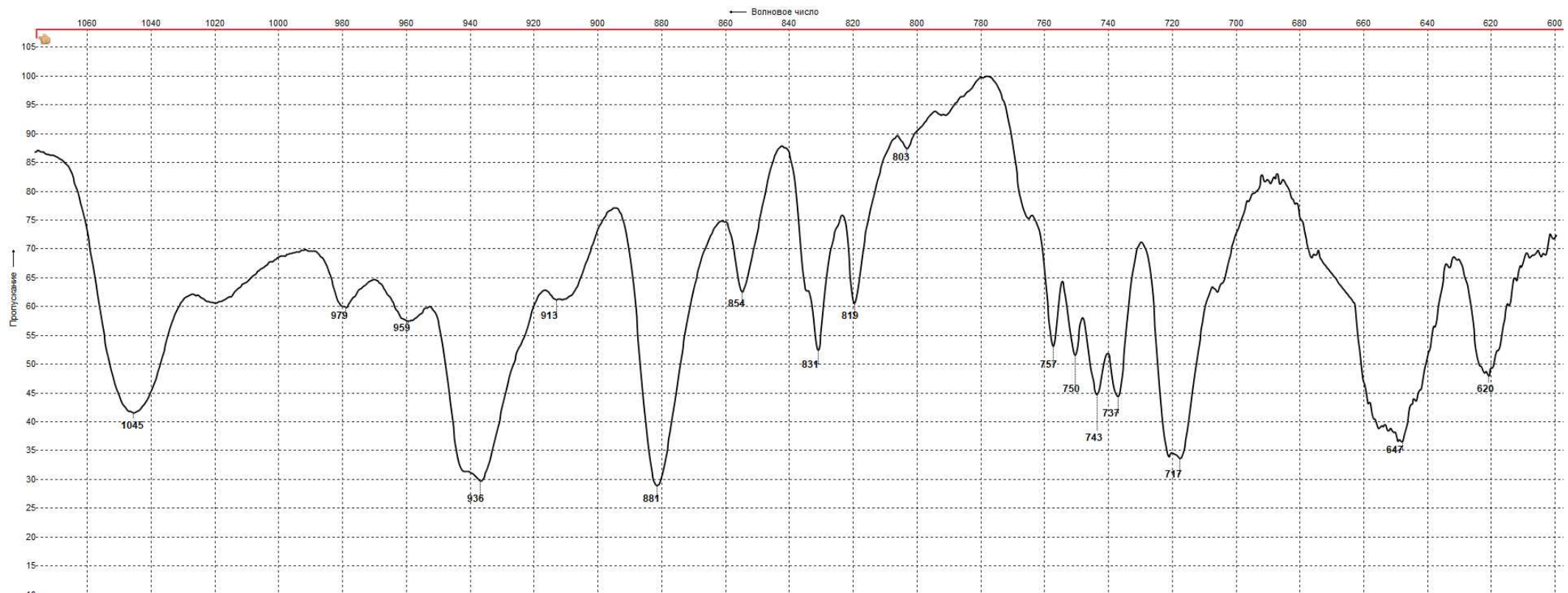
FTIR-ATR spectrum of mixture ϵ -CL-20 with β -CL-20 (3200-600 cm^{-1} range)



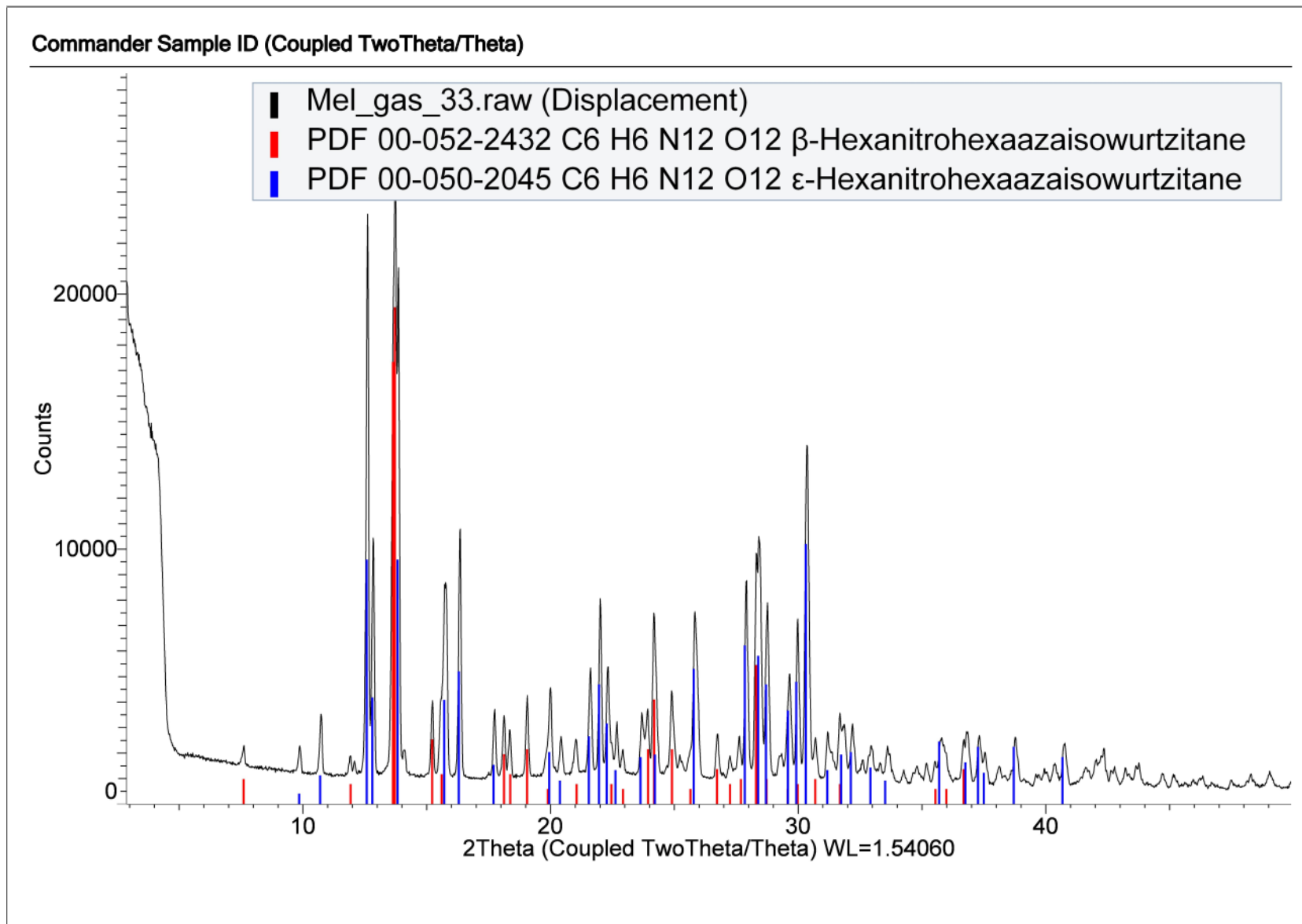
FTIR-ATR spectrum of mixture ϵ -CL-20 with β -CL-20 (1700-600 cm⁻¹ range)

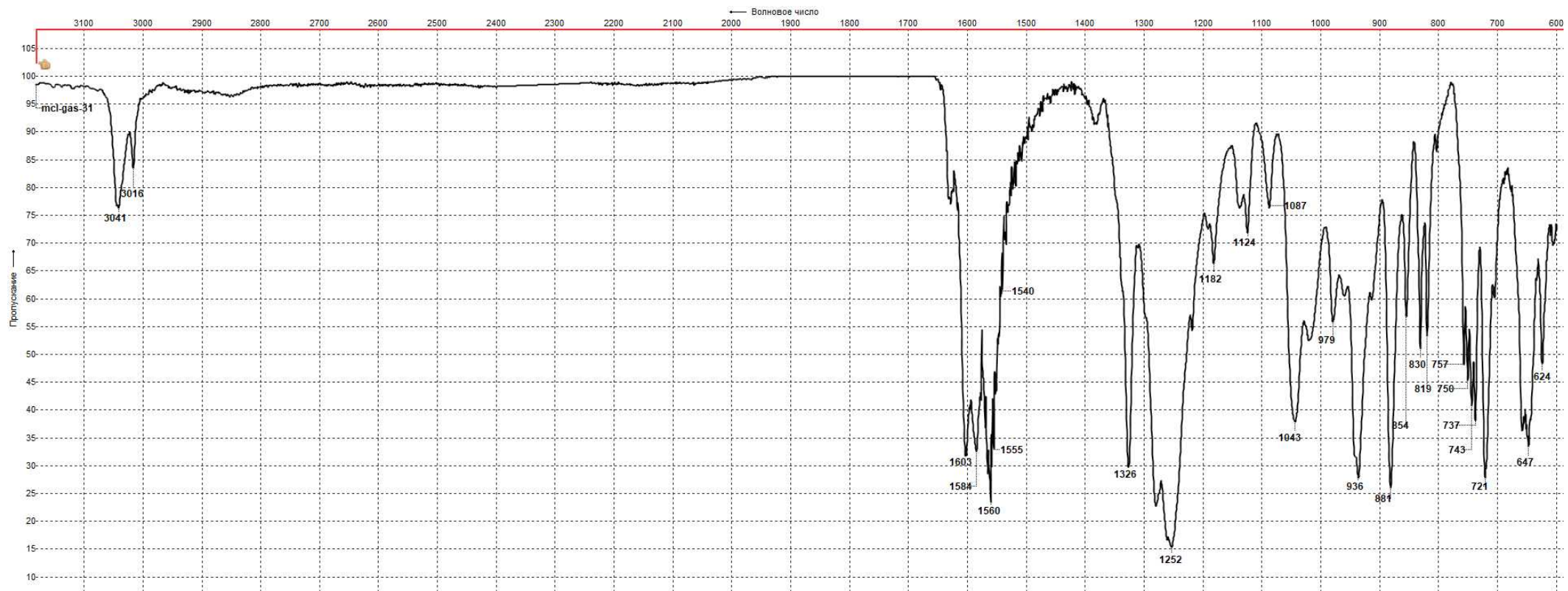


FTIR-ATR spectrum of mixture ϵ -CL-20 with β -CL-20 (1100-600 cm⁻¹ range)

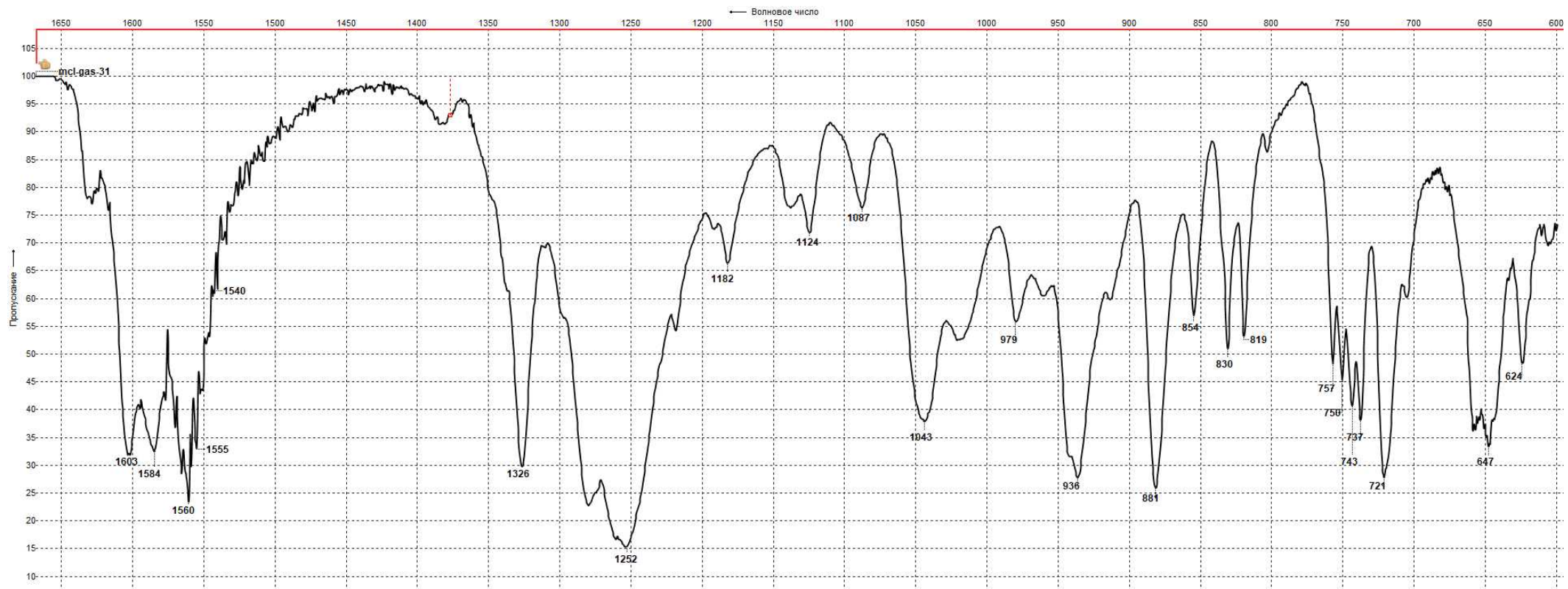


The Powder X-ray diffractogram of mixture ε -CL-20 with β -CL-20

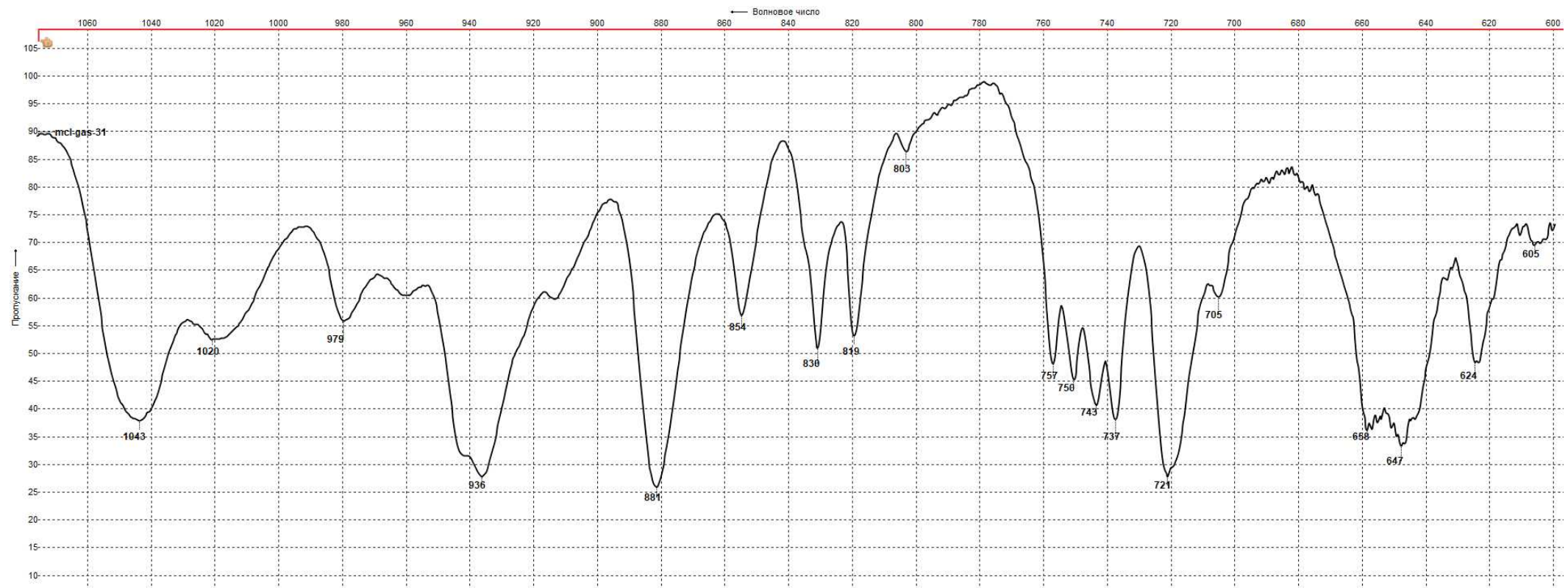


FTIR-ATR spectrum of ϵ -CL-20 (3200-600 cm^{-1} range)

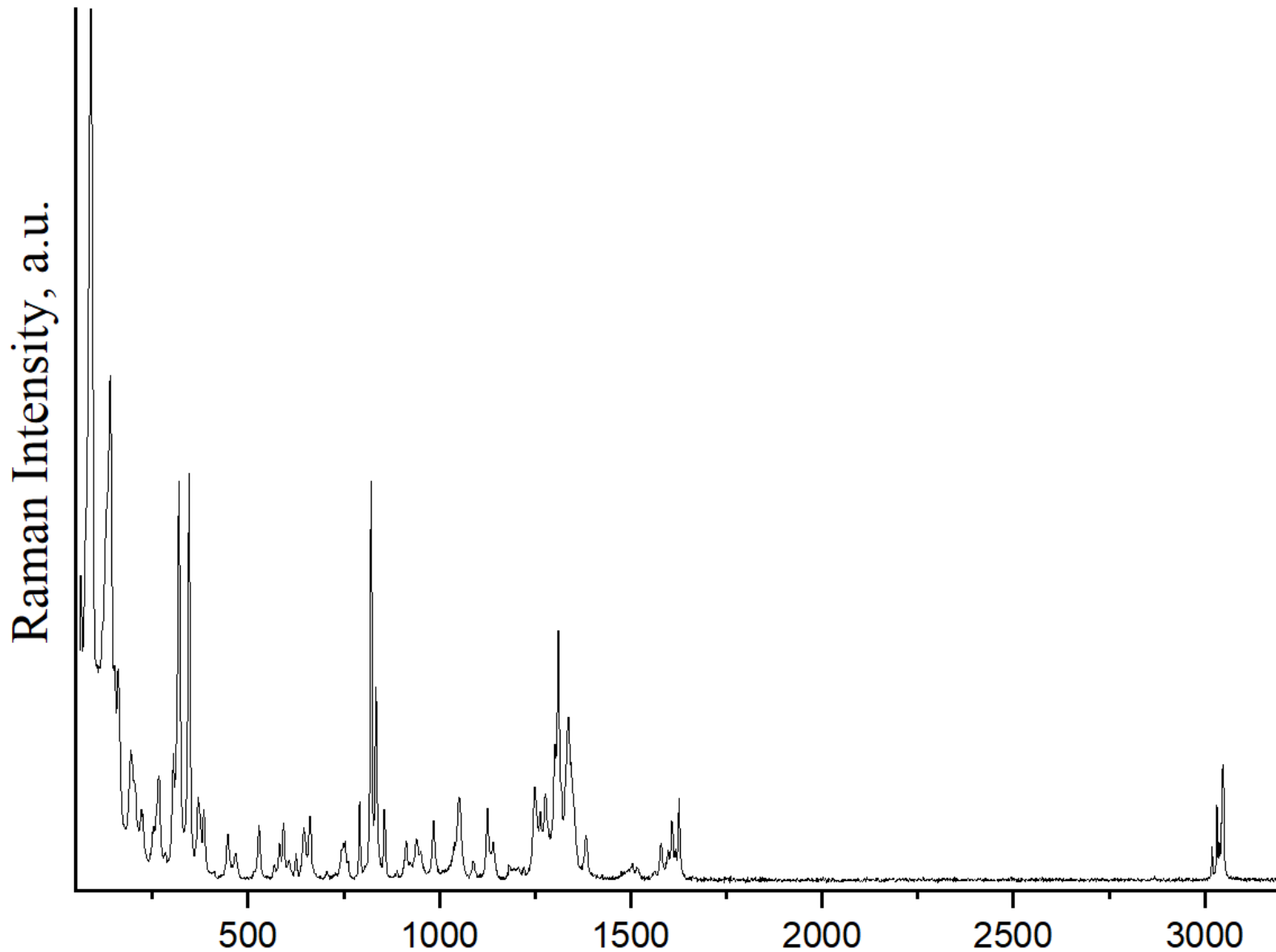
FTIR-ATR spectrum of ϵ -CL-20 (1700-600 cm^{-1} range)



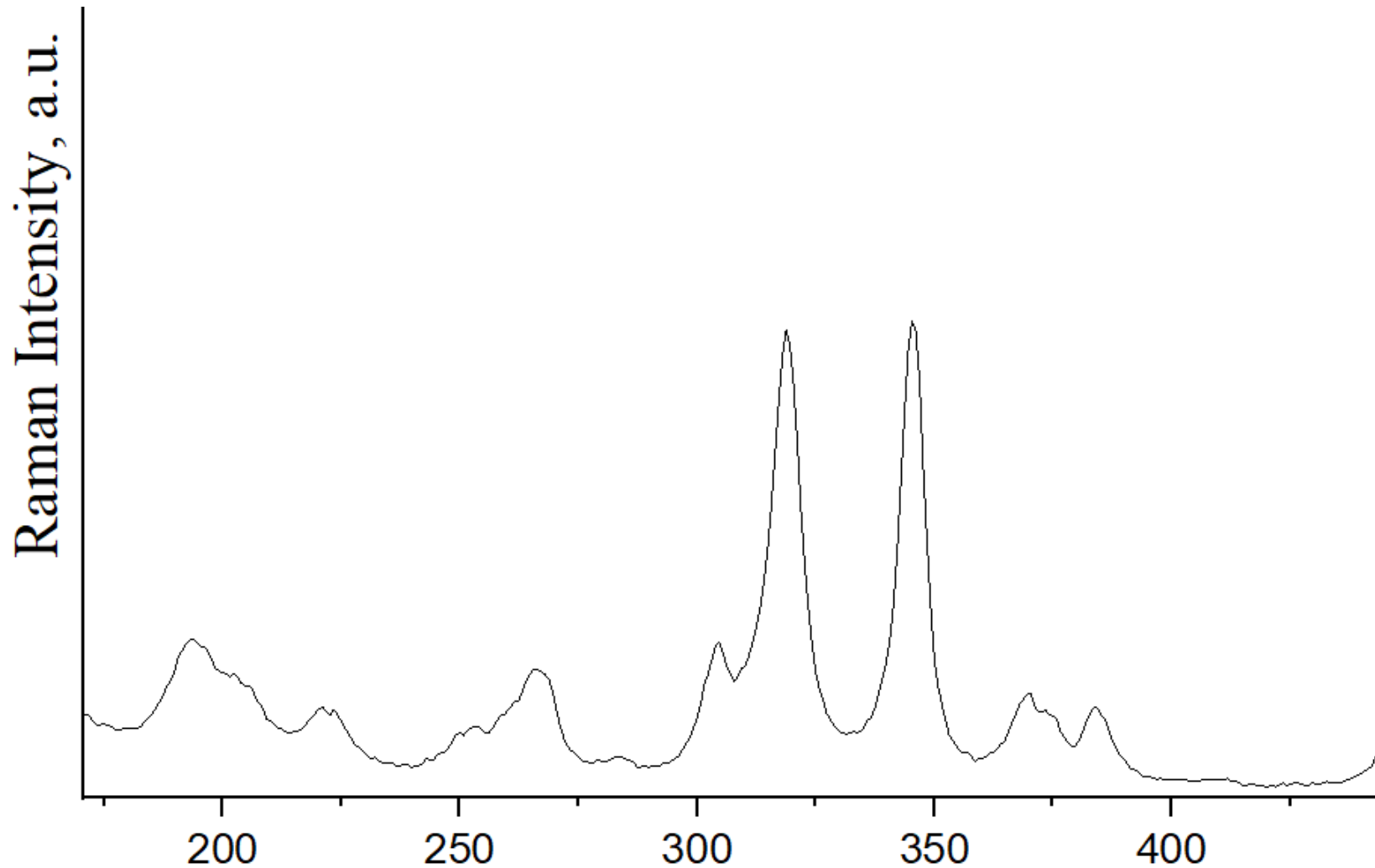
FTIR-ATR spectrum of ϵ -CL-20 (1100-600 cm^{-1} range)

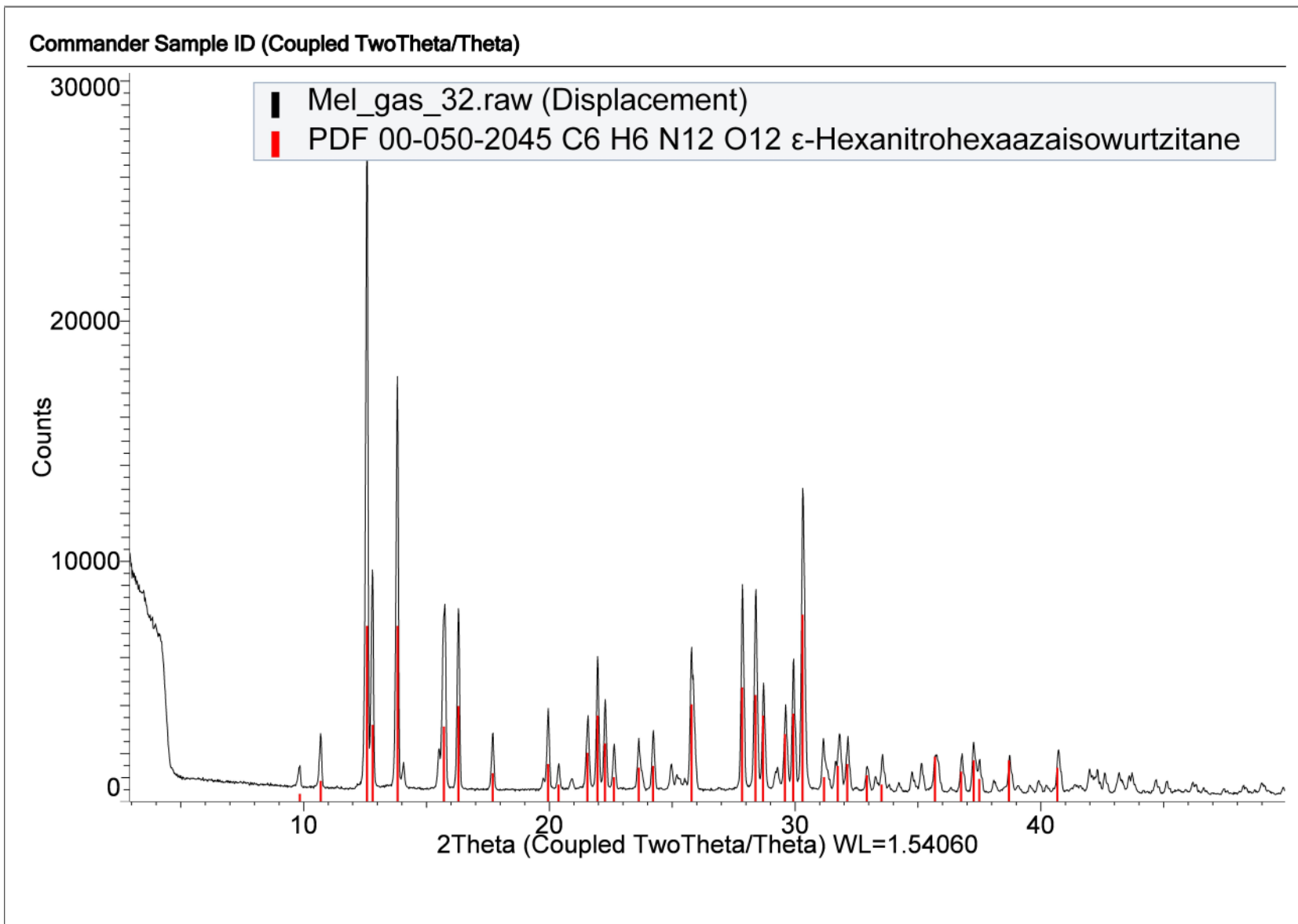


Raman spectrum of ε -CL-20 (0-3500 cm^{-1} range)



Raman spectrum of ϵ -CL-20 (200-400 cm^{-1} range)



The Powder X-ray diffractogram of ε -CL-20

4 Physical-chemical analysis

4.1 Mechanical sensitivity

Table 4. Mechanical sensitivity of the obtained ε -CL-20 particles

Structure	$T_{dec}^b / ^\circ\text{C}$	IS ^c / J	FS ^d / N
Micronized ε -CL-20	229	5.3 ± 0.9	97 ± 19
Original CL-20 powder, $<\text{D}>=120 \mu\text{m}$	229	6.8 ± 2.5	108 ± 34

Impact sensitivity and friction sensitivity of micronized CL-20 sample agrees with that value for raw CL-20.

4.2 Particle size

Laser diffraction analysis revealed the particle size distribution for the micronized sample ε -CL-20 (Figure 4). The mean mass diameter D_{43} dropped to 12 microns after processing.

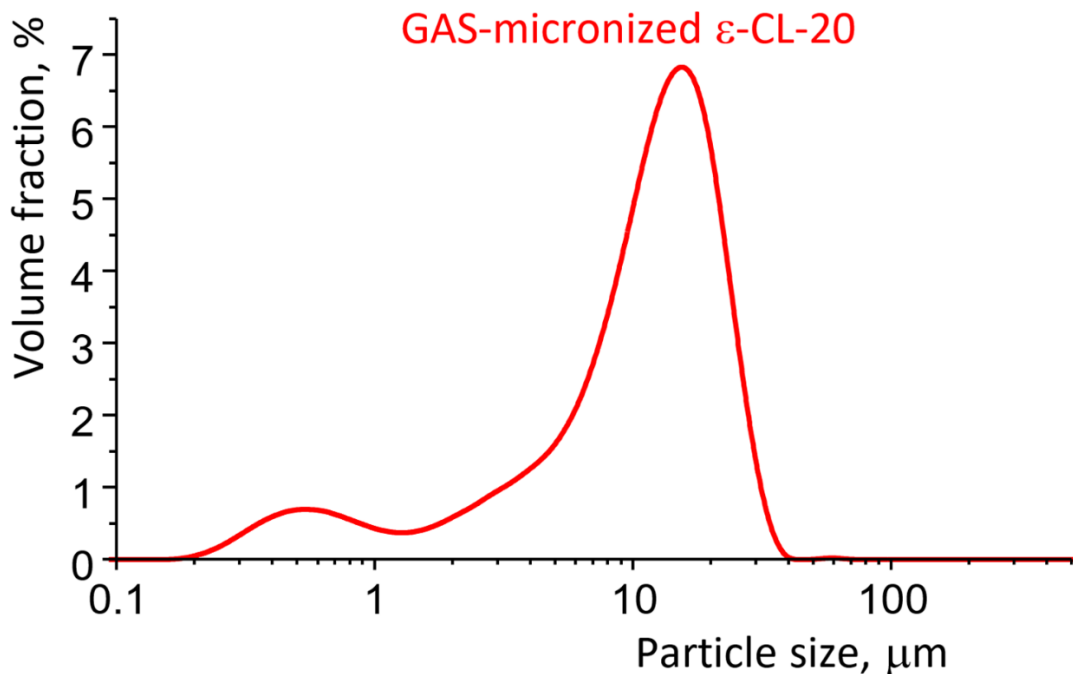


Figure 4. Particle size distribution of micronized ε -CL-20 powder.

4.3 Thermal behavior

Thermal behavior studied using Netzsch DSC 204 HP under nitrogen flow. Sample loads ~0.3 mg for decomposition studies and ~15 mg for observation of phase transition were placed in closed aluminum crucibles with pierced lids and heated linearly with 5 K/min rate up to 300

°C. Impact and friction sensitivity were evaluated according to STANAG procedures in series of 25-30 tests^{9,10}. Resulting values are the drop energy or friction force than correspond to initiation probability of 50%.

Thermal behavior of both CL-20 samples reveals the phase transition with the following exothermic decomposition. The extrapolated onset decomposition temperatures coincide well at 229°C. However, the phase transition for micronized powder is shifted to lower temperatures, i.e., 156°C compared to 164°C for raw CL-20.

DSC /(mW/mg)

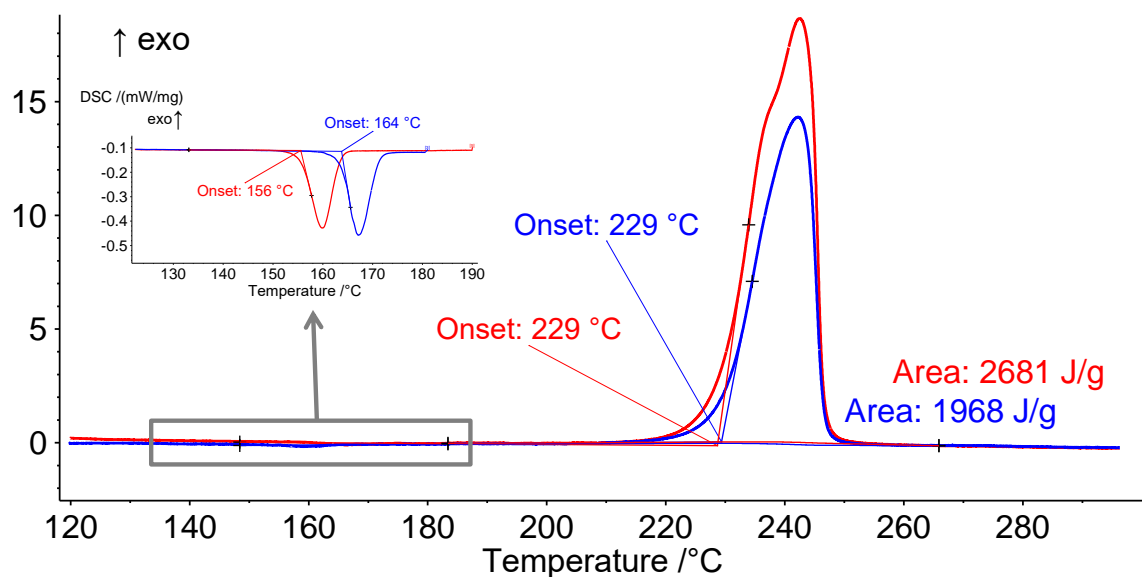


Figure 5. DSC data for micronized (red curves) and raw CL-20 samples under heating at 5 K min⁻¹. Inset shows the magnified phase transition region.

⁹ STANAG 4489, Explosives, Impact Sensitivity Tests, NATO, Brussels, 1999.

¹⁰ STANAG 4487, Explosives, Friction Sensitivity Tests, NATO, Brussels, 2002.

5 X-ray crystallographic data of α -CL-20-CO₂

Since crystals of $(C_6H_6N_{12}O_{12}) \bullet n(L)$ ($n=0.5$, $L=H_2O_2$, the CSD refcode AZAMIZ, CCDC number 1495519;¹¹ $n=0.57$, $L=H_2O$, FEFTRIS, CCDC 260026;¹² $n=0.33$, $L=H_2O$, ILEJUG, CCDC 1406426;¹³ $n=0.25$, $L=H_2O$, PUBMII / PUBMII01 / PUBMII02, CCDC 117776 / 124947 / 1495521;⁹ $n=0.5$, $L=N_2O$, JIYDAZ, CCDC 1585914;¹⁴ $n=0.5$, $L=CO_2$, OLADAH/OLADAH01, CCDC 771863/1585915;^{13,15} have very similar unit cell parameters but include different small molecules L, additionally tree crystals were analyzed by the fast ϕ -scan technique. Structure solutions and the electron density difference map analysis for all specimen undoubtedly confirmed that the structure contains 0.5CO₂ (structures OLADAH and OLADAH01).

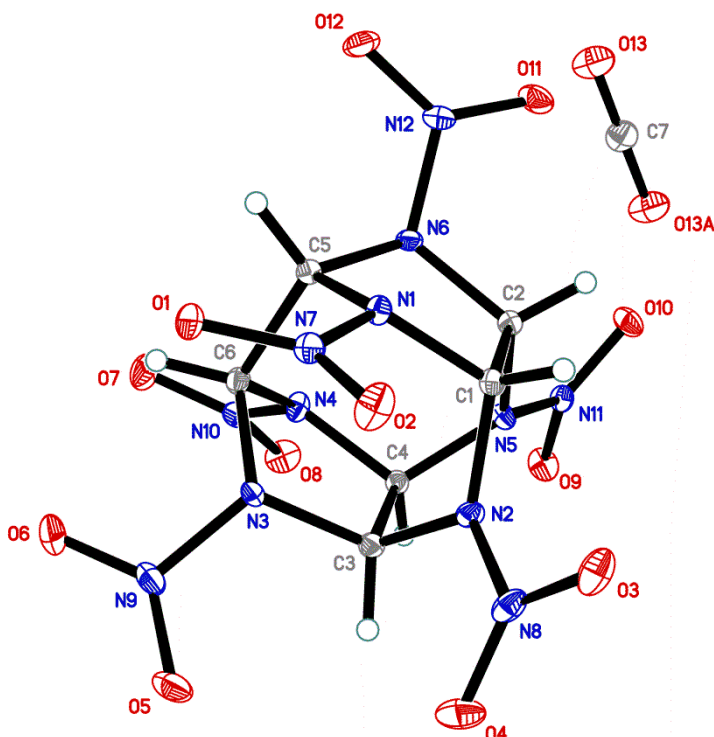


Figure 6. The general view of α -CL-20-CO₂.

¹¹ J.C. Bennion, N. Chowdhury, J.W. A. J. Kampf, Matzger. *Angew. Chem.*, 2016, 128(42), 13312-13315.

¹² N.I.Golovina, A.V.Raevsky, N.V.Chukanov, B.L.Korsunsky, L.O.Atovmyan, S.M.Aldoshin. *Rossisky Khimicheskiy Zhurnal*, 2004, 48, 41-1.

¹³ Y. Yu, S. Jin, J. Zhu, L. Li, S. Chen, Q. Shu. *Z. Kristallogr. - New Cryst. Struct.*, 2016, 231(2), 491-492.

¹⁴ J. Xu, S. Zheng, S. Huang, Y. Tian, Y. Liu, H. Zhang, J. Sun. *Chem. Commun.*, 2019, 55(7), 909-912.

¹⁵ S. Saint Martin, S. Marre, P. Guionneau, F. Cansell, J. Renouard, V.Marchetto, C. Aymonier. *Chem. - Eur. J.*, 2010, 16(45), 13473-13478.

Table 5. Crystal data and structure refinement for α -CL-20-CO₂.

Identification code	MCL12
Empirical formula	C _{6.50} H ₆ N ₁₂ O ₁₃
Formula weight	460.23
Temperature	100(2) K
Wavelength	0.71073 Å
Crystal system	Orthorhombic
Space group	Pbca
Unit cell dimensions	a = 9.61490(10) Å (β = 90°) b = 13.07830(10) Å (β = 90°) c = 23.3712(3) Å (β = 90°)
Volume	2938.85(5) Å ³
Z	8
Density (calculated)	2.080 g/cm ³
Absorption coefficient	0.200 mm ⁻¹
F(000)	1864
Crystal size	0.26 x 0.21 x 0.15 mm ³
Theta range for data collection	2.743 to 36.325°.
Index ranges	-16 <= h <= 16, -21 <= k <= 21, -38 <= l <= 38
Reflections collected	145739
Independent reflections	7114 [R(int) = 0.0285]
Observed reflections	6553
Completeness to theta = 25.242°	99.8 %
Absorption correction	Semi-empirical from equivalents
Max. and min. transmission	0.7474 and 0.7250
Refinement method	Full-matrix least-squares on F ²
Data / restraints / parameters	7114 / 0 / 313
Goodness-of-fit on F ²	1.102
Final R indices [$I > 2\sigma(I)$]	R1 = 0.0282, wR2 = 0.0733
R indices (all data)	R1 = 0.0314, wR2 = 0.0762
Largest diff. peak and hole	0.459 and -0.332 e.Å ⁻³

Table 6. Atomic coordinates ($\times 10^4$) and equivalent isotropic displacement parameters ($\text{\AA}^2 \times 10^3$) for MCL12. U(eq) is defined as one third of the trace of the orthogonalized U^{ij} tensor.

	x	y	z	U(eq)
O(1)	6969(1)	4274(1)	2533(1)	12(1)
O(2)	5853(1)	2922(1)	2226(1)	16(1)
O(3)	4512(1)	1122(1)	2651(1)	16(1)
O(4)	6284(1)	740(1)	3190(1)	21(1)
O(5)	8768(1)	2126(1)	3709(1)	17(1)
O(6)	9122(1)	3755(1)	3841(1)	21(1)
O(7)	7056(1)	5049(1)	4849(1)	16(1)
O(8)	5897(1)	3891(1)	5326(1)	15(1)
O(9)	3096(1)	2578(1)	5088(1)	13(1)
O(10)	1564(1)	3225(1)	4504(1)	13(1)
O(11)	1711(1)	5106(1)	3668(1)	15(1)
O(12)	3382(1)	6101(1)	3371(1)	15(1)
N(1)	4980(1)	3821(1)	2943(1)	8(1)
N(2)	5024(1)	2129(1)	3391(1)	9(1)
N(3)	6953(1)	3200(1)	3634(1)	9(1)
N(4)	5755(1)	3926(1)	4379(1)	9(1)
N(5)	3711(1)	2920(1)	4188(1)	8(1)
N(6)	3890(1)	4519(1)	3687(1)	8(1)
N(7)	6007(1)	3661(1)	2544(1)	9(1)
N(8)	5307(1)	1273(1)	3045(1)	12(1)
N(9)	8403(1)	3010(1)	3749(1)	12(1)
N(10)	6292(1)	4301(1)	4886(1)	10(1)
N(11)	2723(1)	2926(1)	4626(1)	9(1)
N(12)	2916(1)	5300(1)	3553(1)	10(1)
C(1)	4176(1)	2940(1)	3161(1)	8(1)
C(2)	3365(1)	3462(1)	3666(1)	8(1)
C(3)	5994(1)	2394(1)	3835(1)	9(1)
C(4)	5166(1)	2895(1)	4347(1)	8(1)
C(5)	5232(1)	4556(1)	3404(1)	8(1)
C(6)	6407(1)	4182(1)	3835(1)	9(1)
O(13)	85(1)	5620(1)	4649(1)	21(1)
C(7)	0	5000	5000	16(1)

Table 7. Bond lengths [Å] and angles [°] for MCL12.

O(1)-N(7)	1.2241(7)
O(2)-N(7)	1.2277(7)
O(3)-N(8)	1.2135(8)
O(4)-N(8)	1.2174(8)
O(5)-N(9)	1.2132(8)
O(6)-N(9)	1.2130(8)
O(7)-N(10)	1.2259(7)
O(8)-N(10)	1.2210(7)
O(9)-N(11)	1.2266(7)
O(10)-N(11)	1.2146(7)
O(11)-N(12)	1.2159(7)
O(12)-N(12)	1.2158(7)
N(1)-N(7)	1.3741(7)
N(1)-C(5)	1.4636(7)
N(1)-C(1)	1.4786(7)
N(2)-N(8)	1.4075(7)
N(2)-C(3)	1.4372(8)
N(2)-C(1)	1.4419(8)
N(3)-N(9)	1.4412(7)
N(3)-C(6)	1.4648(8)
N(3)-C(3)	1.4769(8)
N(4)-N(10)	1.3825(7)
N(4)-C(6)	1.4561(8)
N(4)-C(4)	1.4639(8)
N(5)-N(11)	1.3959(7)
N(5)-C(4)	1.4483(7)
N(5)-C(2)	1.4486(7)
N(6)-N(12)	1.4208(7)
N(6)-C(5)	1.4509(7)
N(6)-C(2)	1.4732(8)
C(1)-C(2)	1.5710(8)
C(1)-H(1)	0.947(12)
C(2)-H(2)	0.958(12)
C(3)-C(4)	1.5783(8)
C(3)-H(3)	0.930(12)
C(4)-H(4)	0.952(11)
C(5)-C(6)	1.5920(8)
C(5)-H(5)	0.954(12)
C(6)-H(6)	0.945(11)
O(13)-C(7)	1.1570(6)
N(7)-N(1)-C(5)	118.75(5)
N(7)-N(1)-C(1)	119.40(5)
C(5)-N(1)-C(1)	110.14(4)
N(8)-N(2)-C(3)	118.75(5)
N(8)-N(2)-C(1)	118.74(5)
C(3)-N(2)-C(1)	117.26(5)
N(9)-N(3)-C(6)	115.96(5)

N(9)-N(3)-C(3)	114.99(5)
C(6)-N(3)-C(3)	107.43(4)
N(10)-N(4)-C(6)	120.35(5)
N(10)-N(4)-C(4)	121.04(5)
C(6)-N(4)-C(4)	109.47(4)
N(11)-N(5)-C(4)	118.02(4)
N(11)-N(5)-C(2)	117.23(4)
C(4)-N(5)-C(2)	116.64(4)
N(12)-N(6)-C(5)	117.46(5)
N(12)-N(6)-C(2)	116.17(5)
C(5)-N(6)-C(2)	108.74(4)
O(1)-N(7)-O(2)	126.46(5)
O(1)-N(7)-N(1)	117.16(5)
O(2)-N(7)-N(1)	116.37(5)
O(3)-N(8)-O(4)	127.17(6)
O(3)-N(8)-N(2)	116.31(5)
O(4)-N(8)-N(2)	116.44(6)
O(6)-N(9)-O(5)	127.93(6)
O(6)-N(9)-N(3)	116.49(5)
O(5)-N(9)-N(3)	115.43(5)
O(8)-N(10)-O(7)	126.53(6)
O(8)-N(10)-N(4)	116.73(5)
O(7)-N(10)-N(4)	116.60(5)
O(10)-N(11)-O(9)	126.46(5)
O(10)-N(11)-N(5)	117.00(5)
O(9)-N(11)-N(5)	116.43(5)
O(12)-N(12)-O(11)	127.47(5)
O(12)-N(12)-N(6)	116.93(5)
O(11)-N(12)-N(6)	115.42(5)
N(2)-C(1)-N(1)	113.98(5)
N(2)-C(1)-C(2)	108.67(4)
N(1)-C(1)-C(2)	100.41(4)
N(2)-C(1)-H(1)	109.3(7)
N(1)-C(1)-H(1)	111.0(7)
C(2)-C(1)-H(1)	113.3(7)
N(5)-C(2)-N(6)	110.66(4)
N(5)-C(2)-C(1)	107.80(4)
N(6)-C(2)-C(1)	105.19(4)
N(5)-C(2)-H(2)	109.3(7)
N(6)-C(2)-H(2)	111.2(7)
C(1)-C(2)-H(2)	112.5(7)
N(2)-C(3)-N(3)	110.40(5)
N(2)-C(3)-C(4)	108.66(4)
N(3)-C(3)-C(4)	105.04(4)
N(2)-C(3)-H(3)	108.0(7)
N(3)-C(3)-H(3)	111.1(7)
C(4)-C(3)-H(3)	113.6(7)
N(5)-C(4)-N(4)	111.47(5)

N(5)-C(4)-C(3)	107.60(4)
N(4)-C(4)-C(3)	103.08(4)
N(5)-C(4)-H(4)	109.8(7)
N(4)-C(4)-H(4)	111.9(7)
C(3)-C(4)-H(4)	112.8(7)
N(6)-C(5)-N(1)	99.64(4)
N(6)-C(5)-C(6)	109.34(4)
N(1)-C(5)-C(6)	112.40(4)
N(6)-C(5)-H(5)	111.7(7)
N(1)-C(5)-H(5)	111.9(7)
C(6)-C(5)-H(5)	111.3(7)
N(4)-C(6)-N(3)	103.43(4)
N(4)-C(6)-C(5)	108.56(4)
N(3)-C(6)-C(5)	108.75(4)
N(4)-C(6)-H(6)	113.9(7)
N(3)-C(6)-H(6)	111.8(7)
C(5)-C(6)-H(6)	110.2(7)
O(13)#1-C(7)-O(13)	180.0

Symmetry transformations used to generate equivalent atoms: #1 -x,-y+1,-z+1

Table 8. Anisotropic displacement parameters ($\text{\AA}^2 \times 10^3$) for MCL12. The anisotropic displacement factor exponent takes the form: $-2\pi^2 [h^2 a^*{}^2 U_{11} + \dots + 2 h k a^* b^* U_{12}]$.

	U_{11}	U_{22}	U_{33}	U_{23}	U_{13}	U_{12}
O(1)	10(1)	12(1)	14(1)	2(1)	3(1)	-2(1)
O(2)	20(1)	15(1)	13(1)	-6(1)	6(1)	-4(1)
O(3)	22(1)	14(1)	12(1)	-6(1)	3(1)	-6(1)
O(4)	23(1)	13(1)	25(1)	-4(1)	3(1)	8(1)
O(5)	13(1)	18(1)	20(1)	2(1)	2(1)	7(1)
O(6)	10(1)	21(1)	31(1)	4(1)	-4(1)	-4(1)
O(7)	17(1)	14(1)	18(1)	-4(1)	-3(1)	-5(1)
O(8)	21(1)	16(1)	8(1)	-1(1)	0(1)	0(1)
O(9)	13(1)	20(1)	7(1)	4(1)	0(1)	-1(1)
O(10)	8(1)	17(1)	13(1)	2(1)	2(1)	2(1)
O(11)	10(1)	17(1)	17(1)	4(1)	3(1)	4(1)
O(12)	17(1)	9(1)	20(1)	5(1)	1(1)	2(1)
N(1)	8(1)	9(1)	7(1)	-1(1)	2(1)	-1(1)
N(2)	10(1)	7(1)	9(1)	-2(1)	0(1)	1(1)
N(3)	6(1)	10(1)	12(1)	2(1)	0(1)	0(1)
N(4)	11(1)	11(1)	7(1)	0(1)	-2(1)	-3(1)
N(5)	6(1)	11(1)	6(1)	1(1)	1(1)	0(1)
N(6)	8(1)	7(1)	10(1)	1(1)	1(1)	2(1)
N(7)	10(1)	10(1)	8(1)	1(1)	2(1)	0(1)
N(8)	16(1)	8(1)	13(1)	-3(1)	5(1)	-1(1)
N(9)	7(1)	17(1)	12(1)	3(1)	0(1)	1(1)
N(10)	11(1)	11(1)	10(1)	-3(1)	-2(1)	2(1)
N(11)	9(1)	10(1)	8(1)	0(1)	1(1)	-1(1)
N(12)	11(1)	10(1)	9(1)	1(1)	0(1)	4(1)
C(1)	8(1)	9(1)	7(1)	0(1)	0(1)	-1(1)
C(2)	8(1)	8(1)	6(1)	0(1)	0(1)	0(1)
C(3)	8(1)	8(1)	9(1)	1(1)	1(1)	0(1)
C(4)	7(1)	8(1)	8(1)	0(1)	-1(1)	0(1)
C(5)	9(1)	8(1)	8(1)	0(1)	0(1)	0(1)
C(6)	9(1)	9(1)	9(1)	1(1)	-1(1)	-1(1)
O(13)	25(1)	17(1)	22(1)	4(1)	7(1)	4(1)
C(7)	15(1)	14(1)	18(1)	-3(1)	4(1)	2(1)

Table 9. Hydrogen coordinates ($\times 10^4$) and isotropic displacement parameters ($\text{\AA}^2 \times 10^3$) for MCL12.

	x	y	z	$U(\text{eq})$
H(1)	3584(12)	2672(8)	2874(5)	13(2)
H(2)	2377(12)	3448(9)	3611(5)	13(2)
H(3)	6476(12)	1806(9)	3937(5)	15(3)
H(4)	5277(12)	2531(9)	4696(5)	12(2)
H(5)	5430(12)	5223(9)	3259(5)	16(3)
H(6)	7115(12)	4681(9)	3865(5)	13(2)

Table 10. Torsion angles [°] for MCL12.

C(5)-N(1)-N(7)-O(1)	-13.14(8)
C(1)-N(1)-N(7)-O(1)	-152.61(5)
C(5)-N(1)-N(7)-O(2)	168.05(5)
C(1)-N(1)-N(7)-O(2)	28.58(8)
C(3)-N(2)-N(8)-O(3)	-174.86(5)
C(1)-N(2)-N(8)-O(3)	-21.14(8)
C(3)-N(2)-N(8)-O(4)	8.27(8)
C(1)-N(2)-N(8)-O(4)	161.99(6)
C(6)-N(3)-N(9)-O(6)	-21.03(8)
C(3)-N(3)-N(9)-O(6)	-147.52(6)
C(6)-N(3)-N(9)-O(5)	163.18(5)
C(3)-N(3)-N(9)-O(5)	36.69(7)
C(6)-N(4)-N(10)-O(8)	-164.66(5)
C(4)-N(4)-N(10)-O(8)	-21.22(8)
C(6)-N(4)-N(10)-O(7)	19.32(8)
C(4)-N(4)-N(10)-O(7)	162.77(5)
C(4)-N(5)-N(11)-O(10)	160.31(5)
C(2)-N(5)-N(11)-O(10)	12.62(7)
C(4)-N(5)-N(11)-O(9)	-23.35(7)
C(2)-N(5)-N(11)-O(9)	-171.04(5)
C(5)-N(6)-N(12)-O(12)	-23.60(8)
C(2)-N(6)-N(12)-O(12)	-154.80(5)
C(5)-N(6)-N(12)-O(11)	160.84(5)
C(2)-N(6)-N(12)-O(11)	29.63(7)
N(8)-N(2)-C(1)-N(1)	-98.99(6)
C(3)-N(2)-C(1)-N(1)	55.12(6)
N(8)-N(2)-C(1)-C(2)	149.96(5)
C(3)-N(2)-C(1)-C(2)	-55.94(6)
N(7)-N(1)-C(1)-N(2)	54.23(7)
C(5)-N(1)-C(1)-N(2)	-88.40(5)
N(7)-N(1)-C(1)-C(2)	170.22(5)
C(5)-N(1)-C(1)-C(2)	27.58(5)
N(11)-N(5)-C(2)-N(6)	92.91(6)
C(4)-N(5)-C(2)-N(6)	-55.22(6)
N(11)-N(5)-C(2)-C(1)	-152.56(5)
C(4)-N(5)-C(2)-C(1)	59.31(6)
N(12)-N(6)-C(2)-N(5)	-129.44(5)
C(5)-N(6)-C(2)-N(5)	95.39(5)
N(12)-N(6)-C(2)-C(1)	114.39(5)
C(5)-N(6)-C(2)-C(1)	-20.78(5)
N(2)-C(1)-C(2)-N(5)	-2.12(6)
N(1)-C(1)-C(2)-N(5)	-122.00(5)
N(2)-C(1)-C(2)-N(6)	116.00(5)
N(1)-C(1)-C(2)-N(6)	-3.89(5)
N(8)-N(2)-C(3)-N(3)	96.76(6)
C(1)-N(2)-C(3)-N(3)	-57.34(6)

N(8)-N(2)-C(3)-C(4)	-148.55(5)
C(1)-N(2)-C(3)-C(4)	57.35(6)
N(9)-N(3)-C(3)-N(2)	-132.46(5)
C(6)-N(3)-C(3)-N(2)	96.79(5)
N(9)-N(3)-C(3)-C(4)	110.58(5)
C(6)-N(3)-C(3)-C(4)	-20.17(6)
N(11)-N(5)-C(4)-N(4)	-93.34(6)
C(2)-N(5)-C(4)-N(4)	54.54(6)
N(11)-N(5)-C(4)-C(3)	154.34(5)
C(2)-N(5)-C(4)-C(3)	-57.78(6)
N(10)-N(4)-C(4)-N(5)	118.77(6)
C(6)-N(4)-C(4)-N(5)	-94.27(5)
N(10)-N(4)-C(4)-C(3)	-126.09(5)
C(6)-N(4)-C(4)-C(3)	20.88(6)
N(2)-C(3)-C(4)-N(5)	-0.43(6)
N(3)-C(3)-C(4)-N(5)	117.71(5)
N(2)-C(3)-C(4)-N(4)	-118.33(5)
N(3)-C(3)-C(4)-N(4)	-0.19(5)
N(12)-N(6)-C(5)-N(1)	-98.10(5)
C(2)-N(6)-C(5)-N(1)	36.42(5)
N(12)-N(6)-C(5)-C(6)	143.91(5)
C(2)-N(6)-C(5)-C(6)	-81.57(5)
N(7)-N(1)-C(5)-N(6)	176.83(5)
C(1)-N(1)-C(5)-N(6)	-40.26(5)
N(7)-N(1)-C(5)-C(6)	-67.49(6)
C(1)-N(1)-C(5)-C(6)	75.42(6)
N(10)-N(4)-C(6)-N(3)	113.49(5)
C(4)-N(4)-C(6)-N(3)	-33.74(6)
N(10)-N(4)-C(6)-C(5)	-131.12(5)
C(4)-N(4)-C(6)-C(5)	81.65(5)
N(9)-N(3)-C(6)-N(4)	-97.37(5)
C(3)-N(3)-C(6)-N(4)	32.83(6)
N(9)-N(3)-C(6)-C(5)	147.38(5)
C(3)-N(3)-C(6)-C(5)	-82.42(5)
N(6)-C(5)-C(6)-N(4)	-0.25(6)
N(1)-C(5)-C(6)-N(4)	-109.92(5)
N(6)-C(5)-C(6)-N(3)	111.63(5)
N(1)-C(5)-C(6)-N(3)	1.96(6)

Symmetry transformations used to generate equivalent atoms: #1 -x,-y+1,-z+1.